



Computational insight into the contribution of para-substituents on the reduction potential, proton affinity, and electronic properties of nitrobenzene compounds

Adebayo A. Adeniyi^{1,2} · Jeanet Conradie¹

Received: 27 August 2018 / Accepted: 29 January 2019 / Published online: 26 February 2019
© Springer-Verlag GmbH Germany, part of Springer Nature 2019

Abstract

New insight is provided into the chemistry of 12 para-substituted nitrobenzene compounds, using the high-level computational method G3(MP2) and DFT methods. The results show that the chemical properties of the nitrobenzene molecules, such as reduction potential, ionization energy, proton affinity, pK_a , interaction energy of the fragments, hyperpolarizability, exaltation index, band gap, UV electron excitation, and QTAIM properties, are controlled by the strong coupling between the nitro group (NO_2) and the nature of the various para-substituents via the benzene ring as their conducting link. As the electron donating tendency of the para-substituent increases in the molecules, the electron cloud around the nitro group also increases, resulting in contraction of the N–C bonds and elongation of the N=O bonds, consequently leading to gradually increasing electron conductivity, polarizability, and ionization energy but lower proton affinity, thereby progressively impeding the reduction potential of the molecules. The experimental reduction potential was reproduced to a high degree of accuracy, with a mean absolute deviation (MAD) of 0.048 V, depending on the computational method used and the choice of the free energy circle. Additionally, the experimental electron affinity and proton affinity of the 12 molecules were reproduced to a high degree of accuracy.

Keywords Reduction potential · Electron affinity · Proton affinity · pK_a · QTAIM properties · Hyperpolarizability · NEDA analysis · Electron excitation

Introduction

Researchers have shown interest in the reduction mechanism of nitrobenzene and its protonation to phenylhydroxylamine and aniline for decades [1]. These nitro-aromatic compounds are known to have significant biological applications in drugs, such as antibacterial, antiprotozoal, and anticancer agents [2]. The reduction of the nitro group, redox reactivity,

and radical stability are of significant importance in their biological activity [2, 3].

The *p*-CHO substitution of compounds with low electron affinities (EAs), such as the benzonitrile series, were reported to result in significantly higher EA than with *p*-CN substitution, while the reverse was observed in para-substitution of nitrobenzene compounds, where the *p*-CN substituent instead was found to give a higher EA than *p*-CHO [4–6]. This reverse observation in compounds with low EAs is owing to the π -electron withdrawing effect in relation to the field effect of substituents and was also found to be consistent with the concept of varying resonance demand (degree of π -delocalization of the negative charge into the aryl π -system) of the substituents [6].

Both reduction potential and pK_a values are very important parameters in the subfields of chemistry and biology [2, 7]. In many instances, computational quantum methods are often used to reproduce and provide better insight into the experimental reduction potential [8–11] and pK_a [7, 12, 13] of different compounds. In this study, the chemistry of 12 nitrobenzene derivatives (Fig. 1), whose experimental reduction

Electronic supplementary material The online version of this article (<https://doi.org/10.1007/s00894-019-3946-2>) contains supplementary material, which is available to authorized users.

- ✉ Adebayo A. Adeniyi
AdeniyiAA@ufs.ac.za
- ✉ Jeanet Conradie
conradj@ufs.ac.za

¹ Department of Chemistry, University of the Free State, PO Box 339, Bloemfontein 9300, South Africa

² Department of Chemistry, Federal University of Oye-Ekiti, Oye, Nigeria

potentials have been reported in literature [3], are studied computationally in terms of their reduction potential, proton affinity, pK_a , and other electronic properties. The experimentally measured reduction potential of the 12 molecules decreases (becomes more negative), in going from molecule 1 to molecule 12. Since molecules bonded to strong electron donating groups generally have a lower reduction potential than molecules bonded to electron withdrawing groups, the electron donating tendency of the para-substituents R will be considered as increasing from molecule 1 to 12, i.e., the NO_2 group will be considered the most electron withdrawing group, while the amine groups are electron donating.

Methods

Calculation of reduction potential and electron affinity

In this study, two slightly different thermodynamic cycles (cycle 1 and 2) were used to compute the reduction potentials of the 12 molecules, as shown in Fig. 2.

The reduction potential (E_{cell}) is calculated from the free energy expression of cycle 1 (ΔG_{rxn}), as reported in literature [10]:

$$E_{\text{cell}}(\text{in V}) = \frac{-\Delta G_{\text{rxn}}}{nF} - E_{\text{SHE}} \quad (1)$$

$$E_{\text{cell}}(\text{in V}) = \frac{-\left(\Delta G_{\text{gas}}^0 - \Delta\Delta G_{\text{sol}}\right)}{nF} - E_{\text{SHE}} \quad (2)$$

where

$$\Delta G_{\text{rxn}} = \Delta G_{\text{gas}}^0 - \Delta\Delta G_{\text{sol}}$$

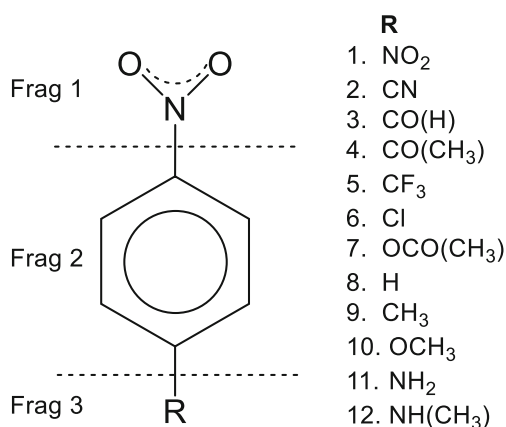


Fig. 1 The schematic representation of the nitrobenzene molecules 1–12, as well as the fragmentation of the molecule into three fragments, for the purpose of natural energy decomposition analysis calculations

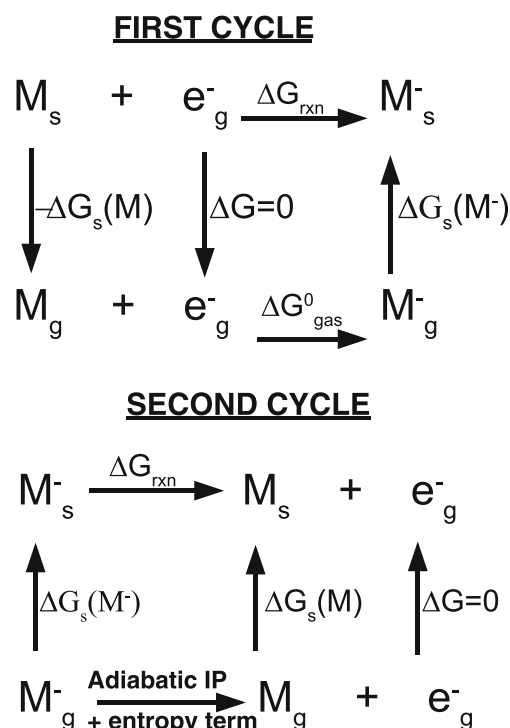


Fig. 2 The schematic representation of the two free energy cycles that were used in this study for the computation of the electrode reduction potentials

In the application of cycle 1 (see Fig. 2), an experimental absolute reduction potential of the Fc/Fc^+ couple ($\text{Fc} = \text{ferrocene}$) in acetonitrile solution (4.980 V) [14] was used as our reference electrode, instead of using E_{SHE} (4.28 V), which is the absolute reduction potential of the standard hydrogen electrode [10]. The values of the two Gibbs free energy terms in Eq. 2 can be expressed as:

$$\Delta\Delta G_{\text{sol}} = \Delta G_s(M^-) - \Delta G_s(M)$$

and

$$\begin{aligned} \Delta G_{\text{gas}}^0 &= G^0(M^-) - G^0(M) \\ &= [U_e(M^-) + ZPE(M^-) + \Delta G_{\text{therm}}(M^-)] \\ &\quad - [U_e(M) + ZPE(M) + \Delta G_{\text{therm}}(M)] \\ &= [H_0(M^-) + \Delta G_{\text{therm}}(M^-)] - [H_0(M) + \Delta G_{\text{therm}}(M)] \\ &= \Delta H_0(M^-) + [\Delta G_{\text{therm}}(M^-) - \Delta G_{\text{therm}}(M)] \\ &= -EA(M) + [\Delta G_{\text{therm}}(M^-) - \Delta G_{\text{therm}}(M)] \\ &= -EA(M) + \Delta\Delta G_{\text{therm}} \end{aligned} \quad (3)$$

ΔG_{therm} in Eq. 4 is the thermal correction to the Gibbs free energy of the reaction in the gas phase, while ΔH_0 is the enthalpy change, with the electron affinity obtained from:

$$\begin{aligned} EA &= -\Delta H_0(M) = H_0(M) - H_0(M^-) \\ &= \{U_e(M) + ZPE(M)\} - \{U_e(M^-) + ZPE(M^-)\} \end{aligned}$$

The accuracy of the electron affinity EA (therefore also the enthalpy change ΔH_0) is very important for the successful reproduction of the reduction potential. In this regard, a

high-level computational method, G3(MP2), which was designed particularly for the prediction of reliable thermochemistry for free radicals [15, 16], was used in this study to compute the EA values. In addition to this expensive high-level G3(MP2) method, different DFT methods were also used, in order to determine the accuracy level in reproducing the experimental reduction properties and electron affinities (EA), when compared with this specialized G3(MP2) method. The G3(MP2) method can become prohibitively expensive as the size of molecules increases, and could be replaced by cheaper DFT methods, if the degree of accuracy proved comparable.

The application of the second cycle (Fig. 2) uses the gas-phase adiabatic ionization energies (IPs) and solvation energies (ΔG) [17] in the following expression:

$$E^0(\text{vs NHE in eV}) = \frac{-\Delta G_{rxn}}{nF} - E_{NHE} \tag{4}$$

$$E^0(\text{vs NHE in eV}) = IP + \frac{-T\Delta S + \Delta\Delta G_{sol}}{nF} - E_{NHE}$$

$$E^0(\text{vs NHE in eV}) = IP + \frac{1}{23.06} \{-T\Delta S + \Delta\Delta G_{sol}\} - E_{NHE}$$

$$E^0(\text{vs NHE in eV}) = IP + \frac{1}{23.06} \{-T\Delta S + \Delta G_s(M) - \Delta G_s(M^{\cdot-})\} - 4.44 \tag{5}$$

IP in the above expression represents the phase adiabatic ionization potential, which is the enthalpy change of one-electron reactions in the gas-phase (either in eV or in V for $1e^-$ transfer); $\Delta G_s(M)$ and $\Delta G_s(M^{\cdot-})$ (both in kcal mol^{-1}) are the solvation effects of the Gibbs free energy; and

ΔS is the gas phase entropy, where 23.06 is the conversion factor for kcal mol^{-1} to V for $1e^-$ transfer.

Further, in the application of cycle 2, the experimental absolute reduction potential of the Fc/Fc^+ couple in acetonitrile solution (4.980 V) [14] was used as our reference electrode, instead of -4.44 V for a normal hydrogen electrode (NHE) [17]. Just as has been applied in the original implementation of the method (for cycle 1), a correction value of 0.28 V was also applied to the reduction potential values in cycle 2, both when using Eq. 5 [17] as well as Eq. 1.

The different approach between cycle 1 and cycle 2 (Fig. 1) is clear when comparing Eqs. 2 and 3 with Eq. 4. In cycle 1

$$\frac{-\Delta G_{gas}^0}{nF} = \frac{EA(M) - \Delta\Delta G_{therm}}{nF}$$

$$= EA(M) + \frac{-\Delta\Delta G_{therm}}{nF} \quad (\text{for EA in V})$$

is used and in cycle 2 the adiabatic IP and entropy term is used $IP + \frac{-T\Delta S}{nF} = -EA + \frac{-T\Delta S}{nF}$ (since in the current case $IP = -EA$).

The microscopic difference in cycle 1 and cycle 2 is thus the difference between the value of the thermal free energy correction $\Delta\Delta G_{therm}$ and the entropy term $-T\Delta S$.

Calculation of pK_a

pK_a is defined as the negative log of the acid dissociation constant, K_a , for the reaction $\text{MH}_s^+ \rightarrow \text{H}_s^+ + \text{M}_s$. The thermodynamic cycle [12] shown in Fig. 3, was used for the computation of the pK_a values of the 12 molecules.

Thus, the $pK_a = -\log K_a$ and can be calculated from the reaction free energy ΔG_{rxn} .

The ΔG_{rxn} is calculated from the gas phase free energy (ΔG_{gas}) and the change in the solvation free energy ($\Delta\Delta G_{sol}$):

$$\Delta G_{rxn} = \Delta G_{gas} + \Delta\Delta G_{sol} \tag{6}$$

The values of ΔG_{gas} and $\Delta\Delta G_{sol}$ were computed from:

$$\Delta G_{gas} = G^0(M_g^{\cdot-}) + G^0(H_g^+) - G^0(MH_g)$$

$$\Delta\Delta G_{sol} = \Delta G(M_s^{\cdot-}) + \Delta G(H_s^+) - \Delta G(MH_s) \tag{7}$$

The gas phase free energy of proton, $G^0(H_g^+)$ was taken as $-6.28 \text{ kcal mol}^{-1}$ [7, 12] and the proton solvation free energy, $\Delta G(H_s^+)$ was taken as $-264.3 \text{ kcal mol}^{-1}$ [18], which falls within the range of 254 to $265 \text{ kcal mol}^{-1}$, confirmed by many different values that have been reported in literature [7, 12, 19, 20]. This large variation range (of 11 kcal mol^{-1} or 0.477 eV) for proton free energy, can by itself introduce an error of up to 8.062 to the computed pK_a value, which is one reason why the accurate prediction of the pK_a is generally regarded as an elusive goal [7], even though the theoretical prediction of pK_a values remains of considerable importance [7]. Liptak and Shields (2001) [12] provided a comprehensive review of the various values of the proton solvation free energy.

Calculation of proton affinity

The computed proton affinity (PA) of the molecules (M) at temperature T, was defined in terms of their gas phase reaction: $\text{M}(g) + \text{H}^+(g) \rightarrow \text{MH}^+(g)$ and was computed from the corresponding enthalpy change [21]:

$$PA(M) = -\Delta H^0(T)$$

$$= \Delta_f H^0(M, T) + \Delta_f H^0(H^+, T) - \Delta_f H^0(MH^+, T) \tag{8}$$

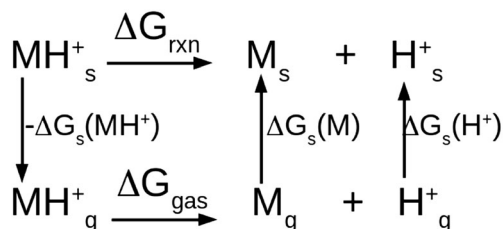


Fig. 3 The schematic representation of the free energy cycle that was used to compute pK_a

The value for the enthalpy of formation of the hydrogen, $\Delta_f H^0(H^+, T)$, was taken as $6.1398 \text{ kJ mol}^{-1}$, as reported in literature [22].

Calculation of molecular dipole, polarizability, and exaltation index

The following are some of the other calculated parameters of the molecules, as used in the static electric field (F) expression:

$$E = E^0 - \mu_i F_i - \frac{1}{2} \alpha_{ij} F_i F_j - \frac{1}{6} \beta_{ijk} F_i F_j F_k - \frac{1}{26} \gamma_{ijkl} F_i F_j F_k F_l \quad (9)$$

- (i) Dipole moment (μ_i), using $\mu = (\mu_x^2 + \mu_y^2 + \mu_z^2)^{1/2}$
- (ii) Linear polarizability tensors (α_{ij}), using:

$$\begin{aligned} \Delta\alpha_1 &= 1/2(\alpha_{xx} + \alpha_{yy}) - \alpha_{zz} \\ \Delta\alpha_2 &= \left\{ 1/2 \left[(\alpha_{xx} - \alpha_{yy})^2 + (\alpha_{xx} - \alpha_{zz})^2 - (\alpha_{yy} - \alpha_{zz})^2 + 6(\alpha_{xy}^2 + \alpha_{xz}^2 + \alpha_{yz}^2) \right] \right\}^{1/2} \\ \Delta\alpha_3 &= \left[(\Delta\alpha_2)^2 - (\Delta\alpha_1)^2 \right]^{1/2} \end{aligned}$$

for the first three polarizabilities α_1 , α_2 , and α_3 [23]

- (iii) Hyperpolarizability (β), namely the first hyperpolarizability tensor (β_{ijk}), using a quasi-pythagorean problem [24, 25], as well as $\beta_{\text{tot}} = (\beta_x^2 + \beta_y^2 + \beta_z^2)^{1/2}$, where:

$$\begin{aligned} \beta_x &= (\beta_{xxx} + \beta_{xyy} + \beta_{xzz}) \\ \beta_y &= (\beta_{yyy} + \beta_{yxx} + \beta_{yzz}) \text{ and} \\ \beta_z &= (\beta_{zxx} + \beta_{zyy} + \beta_{zzz}). \end{aligned}$$

- (iv) The term E^0 in the static energy expression is the energy in the absence of an electronic field, while γ_{ijkl} is the second hyperpolarizability tensor and the i, j , and k labels refer to the x, y , and z components, respectively [26].
- (v) The exaltation index (Γ), expressing the difference in atomic and molecular polarizabilities, calculated by using the expression $\Gamma = \langle \alpha \rangle - \sum_i \langle \alpha \rangle_i$ [23], where $\langle \alpha \rangle = 1/3 (\alpha_{xx} + \alpha_{yy} + \alpha_{zz})$ and where the values of the sum of atomic polarizability of the atoms ($\sum_i \langle \alpha \rangle_i$) were calculated from online data of the atomic polarizability [27].

Natural energy decomposition analysis

The interaction between different fragments in a molecule can be studied, using natural energy decomposition analysis (NEDA):

$$\Delta E = E\psi_{AB} - (E\psi_A + E\psi_B)$$

where ψ_{AB} is the wave function of the AB complex, while ψ_A and ψ_B are the wave functions of the isolated fragments A and B.

The NEDA energy of interaction (ΔE) is then computed, using the five components of the self-consistent field (SCF) interaction energy, as partitioned by the Kitaura and Morokuma method (KM), into the electrostatic (ES), polarization (POL), charge transfer (CT), exchange (XC) energy components, and a coupling term (MIX) [28, 29]:

$$\Delta E = EL + CORE + CT$$

EL in the expression is the electrical energy and CORE refers to the net repulsive components, which are calculated from:

$$\begin{aligned} EL &= ES + POL + SE \\ CORE &= XC + DEF - SE \end{aligned}$$

DEF is the deformation energy of the perturbed wave function and SE is the self-energy correction, which is the polarization penalty. The fragmentation of the molecule into three fragments for the purpose of these NEDA calculations is shown in Fig. 1.

Computational method

The functional B3LYP with the basis set 6-31+G(d) were used for the optimization of the nitrobenzene molecules, in the gas and solvent phases. Acetonitrile was used as solvent medium for the computation of the reduction potentials. Single point energy calculations were done using the ROCCSD(T,FrzG3)/GTBas2 and ROMP2(FrzG3)/GTMP2LargeXP quantum chemical methods, as described for the G3(MP2) method [15, 16]. In this work, a slight modification to the original G3(MP2) method [15, 16] was also applied, namely changing the optimization basis set from 6-31G(d) to 6-31+G(d), as has also been used in a previous report [10]. Further, five additional DFT methods, namely M06/6-311+G(2df,2p), M06/6-311+G(3df,3pd), M06 L/6-311+G(2df,2p), B3LYP/6-311+G(2df,2p), and M06-2X/6-311+G(2df,2p), were also used for single point energy calculations, instead of the high-level computational method G3(MP2), using the same optimized geometries obtained by B3LYP/6-31+G(d). This functional M06 has been reported to be optimal for estimation of thermodynamic parameters [30].

The solvation model based on density (SMD) [31], which is the polarizable continuum model (PCM), was used to compute the free energy of solvation (ΔG_s). The SMD model applies the integral equation formalism variant (IEF-PCM) to solving the nonhomogeneous Poisson equation, with optimized atomic coulomb radii and non-electrostatic terms, from parameters that include solvent accessible surface area as well as atomic and molecular surface tensions [32]. The default parameters were used for the SMD solvation model.

The pK_a and the protonation affinity (PA) of the molecules ($M(g) + H^+(g) \rightarrow MH(g)^+$) were computed in both acetonitrile and aqueous water solution, using the G3(MP2) method and DFT method of B3LYP/6-311+G(df,p), for optimization and solvation energy. The solvation Gibbs free energy (ΔG_s) obtained from G09, was corrected by $\Delta G_s^0 = \Delta G_s + RT \ln(RT/P^0V^0)$ [10], where P^0 and V^0 indicate the values at the standard thermodynamic temperature of 298 K.

Package G09 [33] was used for all calculations of molecular polarizability. Only the natural energy decomposition analysis (NEDA) [29] was obtained by using the NBO 6.0G program [34, 35], which was compiled with GAMESS (US) [36] source code, using the B3LYP/6-311+G(2df,p) method. The rendering of the molecules was done using the packages vmd [37], chimera [38], and AIMAll [39].

Statistical processing

All statistical information from the linear regression Eq. $Y = b_0 + b_1X_1$ were derived using the R statistical package [40]. The quality of the relationship between the derived predictor (X_1) and response (Y) is defined in terms of the quality of the following values:

b_0 (intercept), b_1 (slope), R^2 , F-statistic, residual standard error (RSE), P value, and t -value. The detailed explanation of these statistical parameters is provided in the supplementary information document.

Results and discussion

The B3LYP/6-31+G(d) optimized geometry of each of the molecules is shown in Fig. 4, with the numbering of the atoms.

Electron affinity

The values of the experimental [6, 41–43] and computed electron affinities of the molecules are given in Table 1 and correlated graphically in Fig. 5a. The high-level computational method G3(MP2) produced the best results in reproducing experimental values according to their mean absolute deviation, $MAD = 0.066$ ($MAD = \frac{\sum_1^N |E_{exp} - E_{calc}|}{N}$), while among the

five DFT methods, the best results were obtained by M06/L/6-311+G(2df,2p) ($MAD = 0.160$) and M062X/6-311+G(2df,2p) ($MAD = 0.182$). A high correlation was observed between the experimental and the calculated EA ($R^2 = 0.912 - 0.923$), with p value ranges from $2.65E^{-6}$ to $4.7E^{-6}$, as shown in Fig. 5(a). Among the 12 molecules, only molecule 7 (with substituent p -OCO(CH₃)) has poor alignment in the correlation of the computed EA values with the experimental EA (Fig. 5a).

It is expected that electron affinity and reduction potential should be related, since reduction potential is the potential at which an electron is transferred from the electrode to a neutral molecule (or ion) in solution, while electron affinity is the amount of energy released when an electron is added to a neutral molecule (or ion) in the gaseous state in order to form the negative ion of the molecule (or reduced ion). The correlation between the experimental reduction potentials $E^{0'}$ (Table 2) and the experimental EA values (Table 1) is shown in Fig. 5b (left). A high correlation was indeed observed between the experimental reduction potentials and the experimental EA ($R^2 = 0.906$). The computed EA, using the six different computational methods listed, also significantly correlated with the experimental reduction potentials $E^{0'}$, with R -squared values ranging from $R^2 = 0.984$ to 0.988 (and p -values ranging from $6.49E^{-11}$ to $6.39E^{-6}$), see Fig. 5b (right). However, the values of the computed EA aligned more smoothly with the experimental $E^{0'}$ (Fig. 5b right) than the experimental EA with experimental $E^{0'}$ correlation, in the case where molecules 7 (with p -OCO(CH₃)) and 11 (with substituent p -NH₂) did not align as strongly as the others (Fig. 5b left).

It is very clear from the results of experimental and computational calculated EA values (Table 1) that increasing the electron donation strength of the para-substituent R (in going from molecule 1 to 12 in Fig. 1) results in a lower value of EA, i.e., molecule 12 with the electron donating group NH(CH₃) has a lower affinity for adding an electron than molecule 1 with the electron withdrawing group NO₂. This linear relationship between EA and reduction potential $E^{0'}$ (Fig. 5b) is due to the electronic influence of the R substituent on the energy of the molecule owing to the good electronic communication between the R substituent and the NO₂ group via the benzene ring.

Reduction potential of the molecules

The experimental reduction potential $E^{0'}$ of the nitro group of all the listed nitrobenzenes was characterized as one electron ($1e^-$) reduction, except for molecule 1, which was characterized with two successive one electron ($1e^-$) reduction processes owing to its two NO₂ substituents (dinitrobenzene) [3]. The theoretical reduction potentials were computed from the B3LYP/6-31+G(d) optimized geometries of the molecules

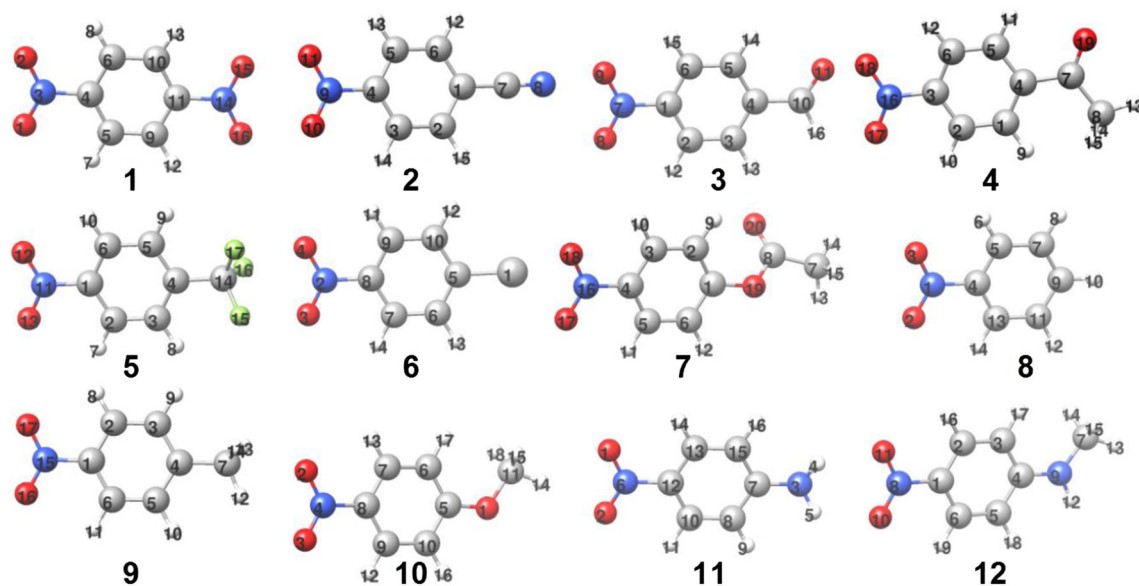


Fig. 4 The 12 B3LYP/6-31+G(d) optimized geometries of the neutral nitrobenzene molecules, showing their atomic numbering

in the neutral and anionic states. Results obtained by using the higher level theory of G3(MP2), as well as the five DFT methods (as outlined in “Atomic electrophilicity and nucleophilicity”), are given in Table 2. The values of the parameters used to compute the reduction potential by the computational methods G3(MP2) and M062x(2df,2p) are in the supplementary material (Table S1).

The degree of accuracy in reproducing the experimental results via calculations, according to their mean absolute deviation (MAD) from the experimental $E^{0'}$ values, are shown in Table 2. Among all the methods, G3(MP2), M06/6-311+G(3df,3pd), and M062x/6-311+G(2df,2p) have the lowest deviation in reproducing the experimental results. The plots

comparing the level of reproduction of the experimental reduction potential $E^{0'}$ at various levels of computational techniques are shown in Fig. 6 for the best four computational methods. The accuracy of reproducing the experimental results was found to depend on the combination of the choice of free energy circle (cycle 1 or cycle 2 in Fig. 2) and the computational methods. The best results when using free energy circle one (Fig. 6(a1) to 6(a3)) was obtained using the high-level G3(MP2) method, with a MAD of 0.067 V (from Table 2). On the other hand, the best level of accuracy when using free energy circle two (Fig. 6(b1) to 6(b3)) for computing the reduction potential was obtained using the DFT method M062X/(6-311+G(2df,2p)), with a MAD of 0.048 V (from

Table 1 The experimental electron affinity (EA in eV) of the molecules, obtained from NIST [41] and other indicated references, as well as the computed EA, using the high-level computational method G3(MP2) and

the five indicated DFT methods. All EA values are given in eV, and the mean absolute deviation (MAD) is stated

	Exp-EA	G3(MP2)	M06(2df,2p)	M06(3df,3pd)	M06 L(2df,2p)	B3LYP(2df,2p)	M062x(2df,2p)
1	2.00 [42]	1.95	2.40	2.36	2.31	2.45	2.25
2	1.72 [42]	1.73	2.02	1.99	1.90	2.05	1.95
3	1.69 [43]	1.66	2.02	1.99	1.95	2.06	1.91
4	1.56 [41]	1.55	1.87	1.85	1.79	1.92	1.77
5	1.50 [43]	1.51	1.75	1.72	1.60	1.81	1.70
6	1.26 [42]	1.29	1.45	1.42	1.28	1.50	1.43
7	1.461 [6]	1.12	1.30	1.28	1.16	1.36	1.25
8	1.01 [42]	1.07	1.22	1.20	1.05	1.26	1.19
9	0.95 [42]	1.00	1.14	1.12	0.96	1.18	1.11
10	0.872 [6]	0.92	1.02	1.00	0.82	1.06	1.01
11	0.915 [6]	0.84	0.87	0.86	0.67	0.93	0.89
12		0.72	0.79	0.77	0.56	0.82	0.78
MAD		0.07	0.23	0.21	0.16	0.26	0.18

Fig. 5 (a) The correlation of the experimental EA (in eV) with computed EA values (graphs are shown for two functionals B3LYP and G3(MP2), and (b) the correlation of the experimental reduction potential $E^{0'}$ (V vs Fc/Fc⁺) with the experimental EA and the computed EA (graph is shown for functional M062x), as obtained from the six different computational methods listed

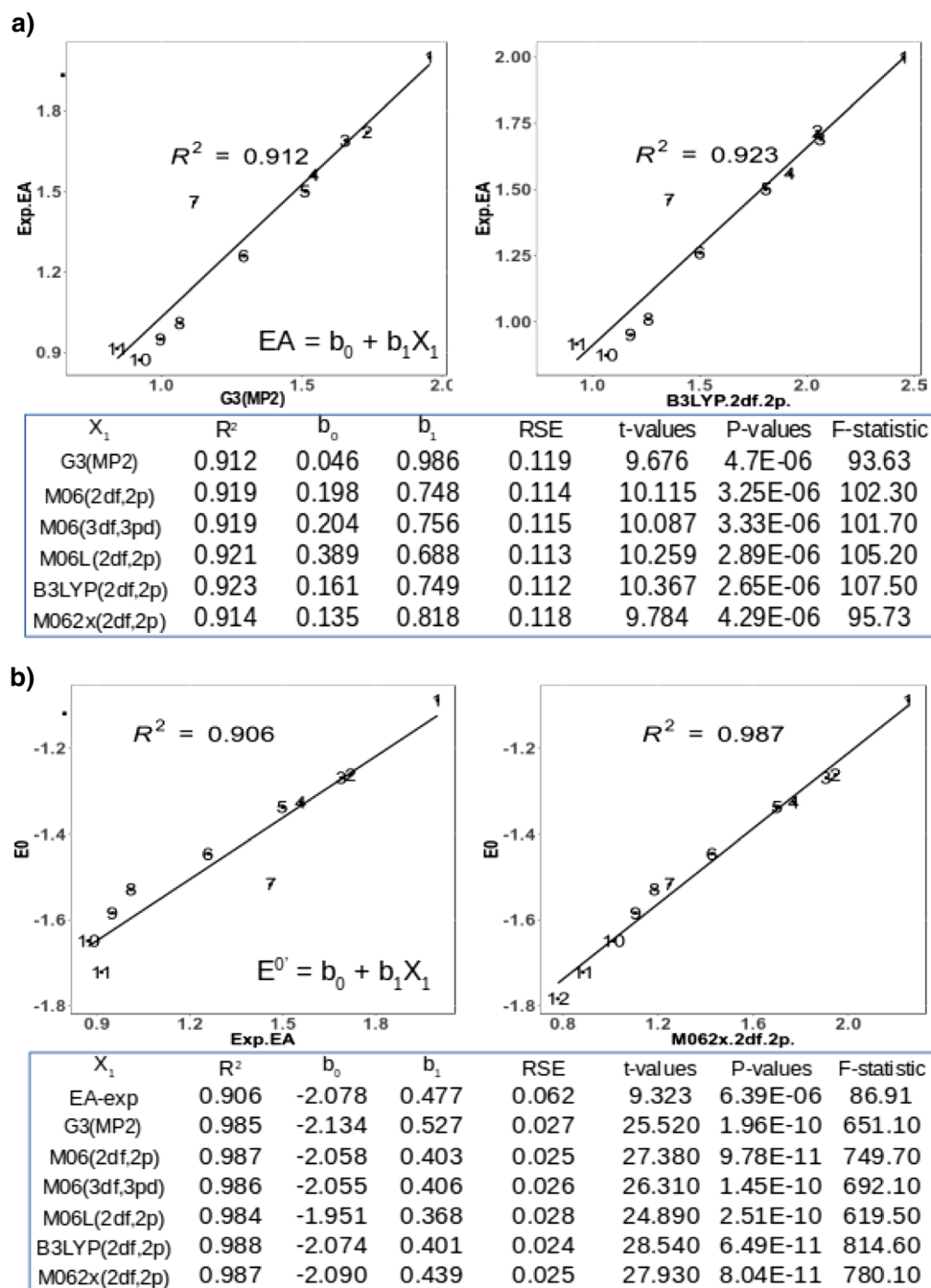


Table 2). A significant improvement in reproducing the experimental reduction potential was observed when the polarization of the basis set 6–311+G was changed from (2df,2p) to (3df,3pd), using the DFT functional M06 (Table 1). In this case, when using cycle 1 the MAD decreased from 0.133 V to 0.115 V, and when using cycle 2 the MAD decreased from 0.092 V to 0.075 V. It follows that the methods G3(MP2) and M062X/6–311+G(2df,2p), which produced the best results in reproducing the experimental potential $E^{0'}$, were also found to best reproduce the experimental EA to a minimal error (“see Conclusions”).

All the molecules from 1 to 12 align strongly with the experimental trend, as shown in Fig. 6(a2) and 6(b2) respectively, for the best methods for cycle 1 and 2. The details of the statistical correlation between the experimental reduction potentials and the computed values are listed in Fig. 6(a3) and 6(b3), when using cycle 1 and cycle 2, respectively. All the computational methods gave a very high level of experimental correlation in a very close range of $R^2 = 0.954$ to $R^2 = 0.990$ (with the p -values significantly low $3.16E^{-12}$ to $5.29E^{-8}$) when using free energy circle 1 (Fig. 6(a3)); while for circle 2 the correlation also was $R^2 = 0.945$ to $R^2 = 0.990$ (with the

Table 2 The experimental reduction potential [3] (E^0 in V versus Fc/Fc^+) and computed reduction potentials of all 12 molecules, using the high-level computational method G3(MP2) as well as five different DFT methods, based on the application of the first and second free energy cycles, as shown in Fig. 2. The basis set 6-311+G was used, together with the specific polarization indicated in brackets for each of the DFT functional methods. All reduction potentials are given in V (versus Fc/Fc^+), and the mean absolute deviation (MAD) is stated

Mol	Exp- E^0	Cycle 1 ^a					Cycle 2 ^a					MAD				
		G3(MP2)	M06(2df,2p)	M06(3df,3pd)	B3LYP(2df,2p)	M062x(2df,2p)	G3(MP2)	M06(2df,2p)	M06(3df,3pd)	M06 L(2df,2p)	B3LYP(2df,2p)		M062x(2df,2p)			
1a	-1.088	-1.226	-0.782	-0.816	-0.728	-0.864	-0.924	-1.283	-0.873	-0.921	-0.873	-0.921	-0.873	-0.921	-0.873	-0.921
1b	-1.233	-1.381	-1.241	-1.272	-1.203	-1.399	-1.314	-1.399	-1.181	-1.437	-1.181	-1.437	-1.181	-1.437	-1.181	-1.437
2	-1.262	-1.316	-1.036	-1.061	-1.003	-1.152	-1.105	-1.380	-1.100	-1.216	-1.125	-1.216	-1.125	-1.216	-1.125	-1.216
3	-1.269	-1.407	-1.052	-1.074	-1.002	-1.157	-1.112	-1.467	-1.112	-1.182	-1.134	-1.182	-1.134	-1.182	-1.134	-1.182
4	-1.326	-1.461	-1.145	-1.165	-1.121	-1.224	-1.244	-1.524	-1.208	-1.288	-1.288	-1.288	-1.288	-1.288	-1.288	-1.288
5	-1.338	-1.438	-1.206	-1.234	-1.149	-1.353	-1.257	-1.518	-1.286	-1.433	-1.314	-1.433	-1.314	-1.433	-1.314	-1.433
6	-1.446	-1.462	-1.311	-1.337	-1.258	-1.479	-1.332	-1.532	-1.381	-1.549	-1.407	-1.549	-1.407	-1.549	-1.407	-1.549
7	-1.517	-1.548	-1.410	-1.431	-1.356	-1.558	-1.465	-1.620	-1.482	-1.630	-1.504	-1.630	-1.504	-1.630	-1.504	-1.630
8	-1.529	-1.526	-1.380	-1.400	-1.338	-1.547	-1.411	-1.605	-1.458	-1.478	-1.478	-1.478	-1.478	-1.478	-1.478	-1.478
9	-1.584	-1.648	-1.513	-1.528	-1.473	-1.686	-1.473	-1.759	-1.624	-1.798	-1.639	-1.798	-1.639	-1.798	-1.639	-1.798
10	-1.649	-1.632	-1.544	-1.565	-1.503	-1.747	-1.554	-1.720	-1.632	-1.834	-1.652	-1.834	-1.652	-1.834	-1.652	-1.834
11	-1.722	-1.709	-1.680	-1.691	-1.624	-1.878	-1.665	-1.792	-1.763	-1.960	-1.774	-1.960	-1.774	-1.960	-1.774	-1.960
12	-1.784	-1.803	-1.740	-1.754	-1.707	-1.966	-1.747	-1.930	-1.866	-2.093	-1.881	-2.093	-1.881	-2.093	-1.881	-2.093
MAD		0.067	0.133	0.115	0.107	0.177	0.091	0.137	0.092	0.146	0.075	0.146	0.075	0.146	0.075	0.146

^a An experimental absolute reduction potential of Fc/Fc^+ in acetonitrile solution (4.98 V) [14] was used, instead of using E_{SHE} (4.28 V) [10] for cycle 1, or instead of using E_{NHE} (-4.44 V) of normal hydrogen electrode (NHE) [17] for cycle 2. All calculated reduction potential values were corrected with 0.28 V, as suggested in the literature [17]

^b Reduction of the second p -NO₂ group of molecule 1

p -values significantly low = 7.69E^{-11} to 1.29E^{-7}), according to Fig. 6(b3). In terms of correlation with the experimental values, the methods M06/6-311+G(2df,2p), M06 L/6-311+G(2df,2p), and B3LYP/6-311+G(2df,2p) gave a higher correlation (R^2), although they have higher deviations (MAD) from the experimental compared to G3(MP2).

The calculated reduction of the second NO₂ group of molecule 1 was significantly lower than the reduction of the first NO₂ group (Table 2), just as was observed experimentally (0.145 V lower experimentally). This is due to electrostatic factors, since the second reduction involves adding an electron to a species that already bears a negative charge, owing to electron communication between the two NO₂ groups via the benzene ring. This renders the second reduction much more difficult than the first reduction [3]. All the computed reduction potentials and experimental reduction potentials demonstrate a very similar pattern of increasing from 1 to 12 in difficulty of reducing the molecule (more negative reduction potential values far from 0.0 V), as the strength of the electron donation increases from molecule 1 (with the electron withdrawing p -NO₂ group) to molecule 12 (with the electron donating p -NH(CH₃) group) (Fig. 6). This hindrance in reduction is owing to the strong electron push from a strongly electron donating R substituent group (Fig. 1) toward the nitro group via the benzene ring, which reduces the susceptibility of the NO₂ to further reduction.

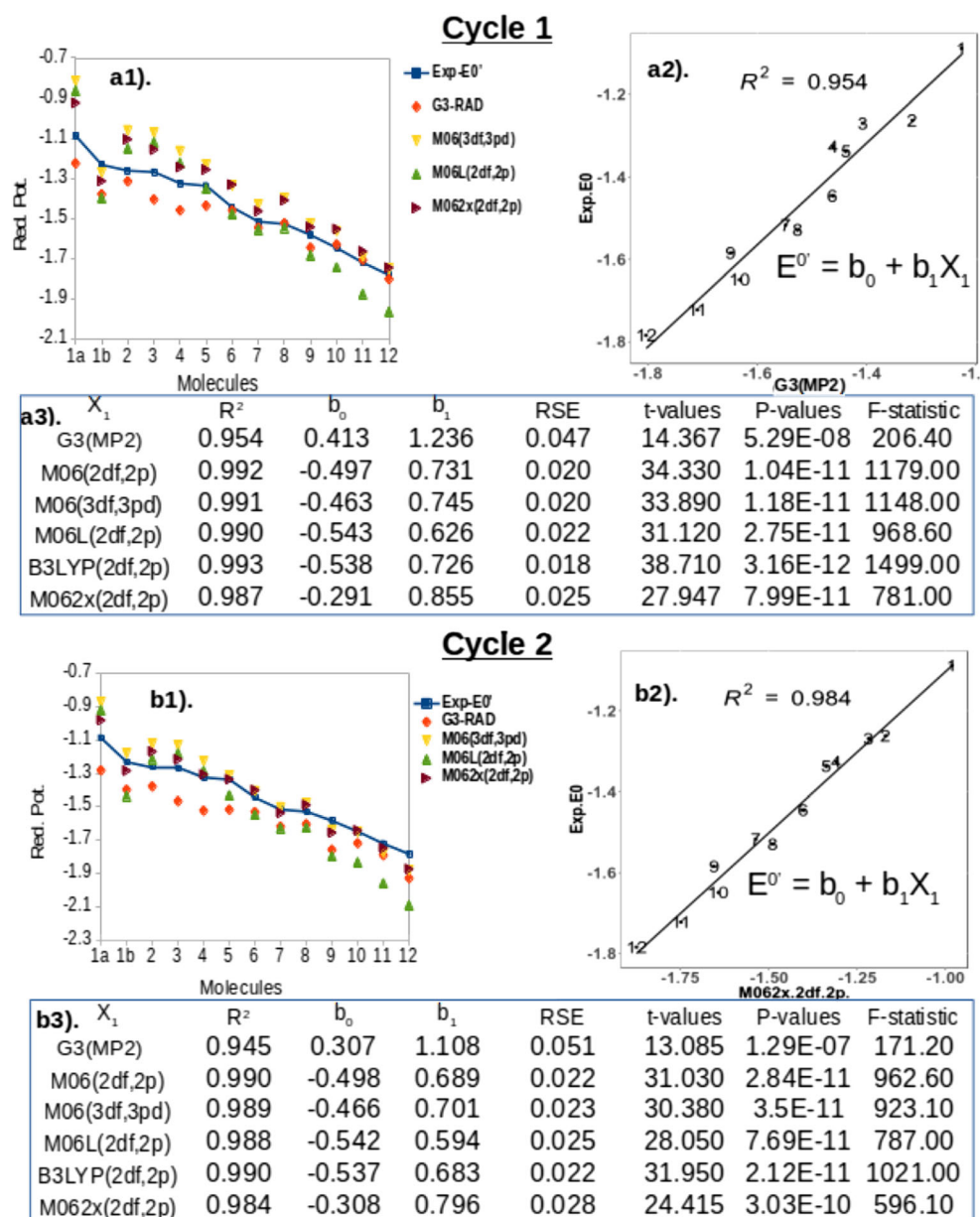
Ionization energy and oxidation potential

Experimental and calculated ionization energy (IE) values are given in Table 3. The computed IE values (from $\text{IE} = \text{H}^0(\text{M}^+) - \text{H}^0(\text{M}) = \{\text{U}^0(\text{M}^+) + \text{ZPE}(\text{M}^+)\} - \{\text{U}^0(\text{M}) + \text{ZPE}(\text{M})\}$) are in very good agreement with the experimental values. The high-level computational method G3(MP2) gives a relatively higher accuracy (MAD = 0.121 eV) when compared to the DFT method M06 L/6-31+G(2df,2p) (MAD = 0.547 eV), as given in Table 3.

It is observed that the experimental reduction potential $E^{0'}$ and the experimental ionization energy (Exp-IE) follow the same trend, as evidenced by the combination of R^2 ($R^2 = 0.779$) and p value (p value = 3.21×10^{-4}), shown in Supplementary Fig. S1a. The reason for the relatively lower correlation of $E^{0'}$ with experimental IE is because of poor alignment of molecule 1 containing two NO₂ groups, compared to the others containing only one NO₂ (Fig. S1a).

It is expected that ionization energy and oxidation potential should also be related, since oxidation potential is the potential at which an electron is transferred from a molecule in solution to the electrode, and ionization energy is the amount of energy needed to remove an electron from a molecule in the gaseous state. Thus, in order to gain insight into the possible oxidation of the molecules, their oxidation potentials were computed (Table S2). A

Fig. 6 (1) Graph of the experimental ($E^{0'}$) and the computed reduction potentials (showing the best four of the computational methods) for the 12 molecules, (2) graph of the correlation of the results of one of the theoretical methods with experimental $E^{0'}$, and (3) a statistical analysis of the correlation between the experimental value and the six different theoretical methods, for (a) when the free energy cycle 1 was used and (b) when the free energy cycle 2 was used. The basis set 6-311+G was used together with various polarizations, as indicated in brackets for each of the DFT functional methods



gradual decrease in the values of the calculated oxidation potentials (Table S2) and IE (Table 3) was observed from molecule 1 to 12. The computed oxidation potentials highly correlated with the experimental IE ($R^2 = 0.943$ to 0.949 , p value = 3.90×10^{-7} to 6.46×10^{-7}) (Fig. 7). Since a molecule with a higher electron donation tendency of the para-substituent (such as 12, with $p\text{NH}(\text{CH}_3)$) has a lower ionization energy IE, it consequentially also has a lower oxidation potential.

Statistically, there is also a reasonable correlation obtained between the experimental reduction potential $E^{0'}$ and the computed oxidation potential ($R^2 = 0.728$ to 0.789 , p value = 2.60×10^{-4} to 4.18×10^{-4}) (Fig. S2). Many of the computed oxidation potentials of the molecules aligned strongly with the

experimental reduction potential $E^{0'}$, except for molecule 1 (with $p\text{-NO}_2$). It is obvious from the results that molecules like 1, with a higher tendency toward reduction (less negative reduction potential), have a lower tendency toward oxidation and are consequentially characterized with higher oxidation potentials (Fig. S2) and IE (Fig. S1a).

Proton affinity

The protonation of compounds like nitrobenzene, aniline, and benzaldehyde are known to take place at the substituent itself, unlike protonation of compounds like toluene, bromobenzene, biphenyl, and iodobenzene, which takes place on the ring [44]. Therefore, the proton affinities of the nitrobenzene

Table 3 The experimental (obtained from NIST database [41]) and computed ionization energy (IE) at 298 K. All values are given in eV, and the mean absolute deviation (MAD) is stated

	Exp-IE	G3(MP2)	M06 L(2df,2p)
1	10.30	10.60	10.11
2	10.59	10.49	9.75
3	10.27	10.27	9.52
4	10.07	10.02	9.13
5			9.81
6	10.00	9.82	9.40
7	9.70	9.38	8.83
8	10.16	9.97	9.69
9	9.46	9.63	9.06
10	9.00	9.00	8.66
11	8.60	8.48	8.23
12	8.17	8.16	7.93
MAD		0.12	0.55

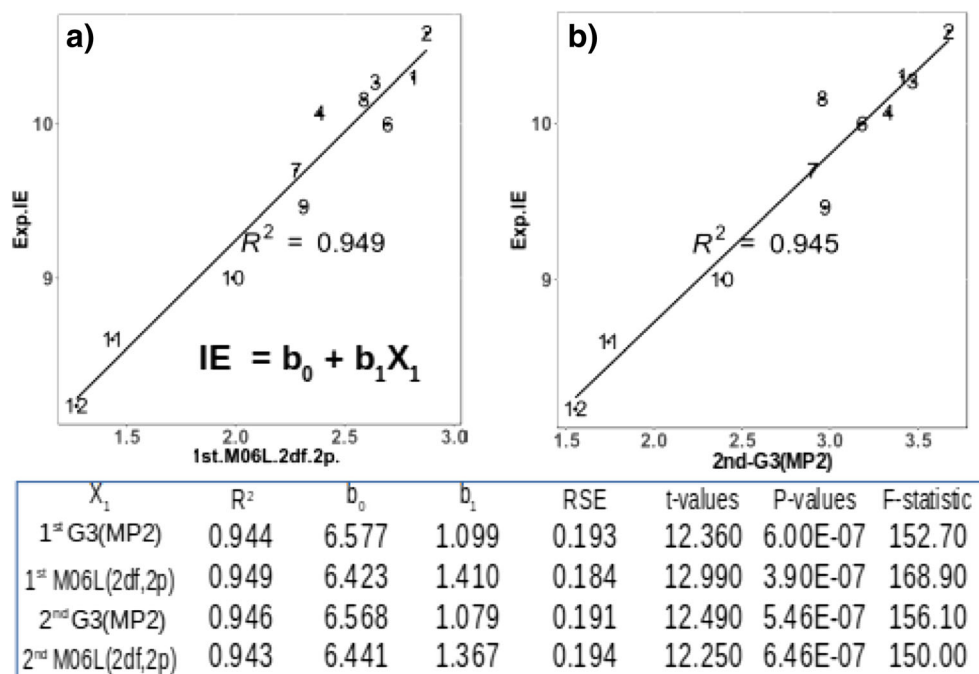
Table 4 The experimental proton affinity obtained from the NIST database [41], and the computed proton affinity obtained by G3(MP2) and B3LYP methods. All values are given in eV, and the mean absolute deviation (MAD) is stated

	Exp-PA	G3(MP2)(df,p)	B3LYP(df,p)
1		7.730	7.780
2	8.040	7.779	7.919
3	8.241	7.962	8.044
4	8.543	8.067	8.177
5		7.888	7.963
6		8.117	8.277
7	8.428	8.345	8.553
8	8.295	8.173	8.288
9	8.449	8.348	8.511
10		8.580	8.766
11	8.975	8.867	9.034
12	9.241	9.033	9.178
MAD		0.205	0.125

molecules in this work were computed by the protonation of one of the oxygen atoms of the NO₂ unit of the molecules (Table 4). The experimental PA values (Table 4) of the molecules were reproduced by DFT computations to a significant level of accuracy, especially when the DFT method B3LYP/6-311+G(df,p) was used (with MAD = 0.125 eV), compared to the high-level G3(MP2) method (with MAD = 0.205 eV).

The experimental reduction potentials (E^0) of the molecules show significant correlation ($R^2 = 0.711$) with their

experimental proton affinities (Exp-PA) (Fig. S1b). However, contrary to IE, the proton affinity is in a reverse relation with the reduction potential of the molecules. As the electron cloud around the NO₂ group increases from molecule 1 to 12, owing to the increasing tendency of electron donation of the 12 para-substituents R, the IE of the molecule decreases and the PA increases, which consequentially impedes reduction of the molecule (the reduction potential values are shifted

Fig. 7 The correlation of the experimental IE (eV) with the computed oxidation potential (in V versus SHE), calculated by two different functionals G3(MP2) and M06 L, using both (a) the first (1st) and (b) the second free energy cycles (2nd) in each computation, as listed in the statistical analysis of these correlations

more negative, away from 0 V). The experimental ionization potential (Exp-IE) was also found to be highly correlated with the experimental proton affinity Exp-PA (with $R^2 = 0.927$, p value = $1.27E^{-4}$), as well as correlated with the computed PA, obtained by computational methods G3(MP2) and B3LYP (with $R^2 = 0.932$ to 0.953), see Fig. 8.

pK_a

Another important property that was computed for all 12 molecules, is the pK_a , calculated in both acetonitrile and water media. Limited experimental values are available for the pK_a of the molecules, and therefore the calculated pK_a values (the acid dissociation constant at logarithmic scale of the reaction $MH_s^+ \rightarrow H_s^+ + M_s$) were related to the experimental PA instead (enthalpy change of the reaction $M(g) + H^+(g) \rightarrow MH^+(g)$ from Table 4. The wide range of proton solvation free energy, which alone can introduce an error of up to 8.062 into pK_a as previously discussed, contributes significantly to the reason why accurate computation of the pK_a is also regarded as an elusive goal [7].

The values of the computed pK_a of the molecules, calculated at different levels of theory and in both acetonitrile and water media, are shown in Table 5. Generally, the pK_a values decrease from molecule 1 to 12, indicating an increase in acidity from 1 to 12. A very significant change in the computed pK_a value was observed in the different results, when obtained by different computational methods. For example, there was a marked difference when comparing the G3(MP2) and B3LYP results, or when changing the basis set from 6-31+G(d) to 6-311+G(df,p). Additionally,

the solvent used in the calculations (acetonitrile or water), had a large influence on the computed values. The water medium resulted in much lower calculated pK_a values, when compared to acetonitrile. All the computed values differed significantly from the two available experimental pK_a values, although the two experimental values follow the same trend as the calculated pK_a .

The computed pK_a values were correlated with the experimental proton affinities (Fig. 9) for lack of sufficient experimental pK_a data. The computed pK_a was found to decrease with an increase in experimental PA, while the high-level computational method G3(MP2) produced a better correlation ($R^2 = 0.919$, p value = $1.73E-4$), compared to the DFT method B3LYP ($R^2 = 0.887$, p value = $4.74E-4$). The computed pK_a of the molecules decreases from molecule 1 to 12 as their electron withdrawing tendency decreases (Fig. 9, Table 5), while their proton affinity increases. This systematic decrease in the pK_a is further evidence of very strong electron communication between the para-substituent R and the NO_2 group via the benzene ring, leading to an increase of the electron cloud around the NO_2 owing to the increasing electron donation from molecule 1 to 12.

Atomic electrophilicity and nucleophilicity

The ability of the atoms in the molecules to act as the center for nucleophilic (f^+), electrophilic (f^-) or radical (f^0), attack was examined using Fukui indices. The change in electronic distribution was examined, when changing from the neutral state (N electron system) to the reduced state (N+1) and oxidized state (N-1). Under a constant external potential $v(r)$, the

Fig. 8 The correlation of the experimental ionization energy (Exp-IE in eV) with both (a) experimental proton affinity (Exp-PA) and (b) computed proton affinity (in eV), calculated by two different computational methods G3(MP2) and B3LYP(df,p) for the system, (c) the statistical analysis of these correlations

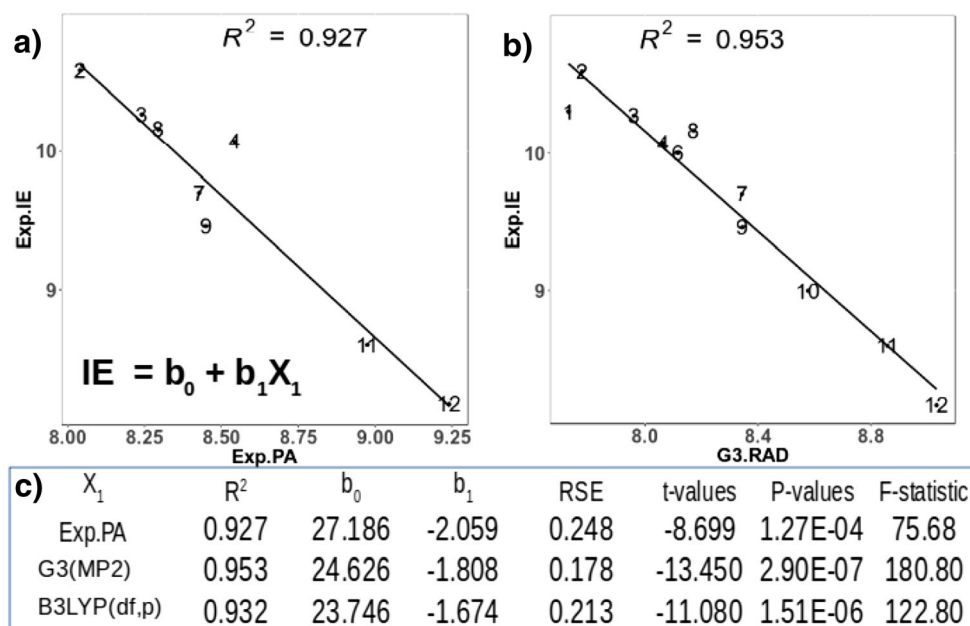


Table 5 The computed pK_a of the molecules in both CH_3CN and water media using G3(MP2) and B3LYP computational methods

	Exp pK_a	CH_3CN medium			Water medium	
		G3(MP2)	B3LYP(d)	B3LYP(df,p)	G3(MP2)	B3LYP(df,p)
1		31.9	27.9	27.4	29.1	23.2
2		32.7	26.9	24.9	28.8	20.9
3		30.7	26.0	24.0	27.5	20.6
4		30.2	25.1	23.0	27.1	19.8
5		33.0	28.8	24.8	27.8	20.9
6		30.4	24.3	22.2	27.4	19.1
7		29.0	22.3	21.0	27.8	18.8
8	3.98 ^a	29.2	23.7	21.7	26.0	18.5
9		28.8	23.1	19.5	25.2	16.9
10		25.4	18.7	16.5	23.5	14.6
11	1.02 ^a	20.6	13.9	11.9	19.5	10.6
12		19.8	13.4	10.9	18.1	9.8

^aThe two experimental pK_a were taken from reference [45]

Fukui indices can be expressed in terms of the change in electronic density $\rho(r)$, with respect to the change in the number of electrons (N) [46]:

$$f(r) = \left(\frac{\partial \rho}{\partial N} \right)_v$$

A higher positive value of the Fukui function (f_j) of an atom in a molecule is an indication that the atom will act as the center for higher nucleophilic (f^+), electrophilic (f^-) or radical attack (f^0) [47]. The site with the highest value of a Fukui index indicates a high reactivity, though in some cases it

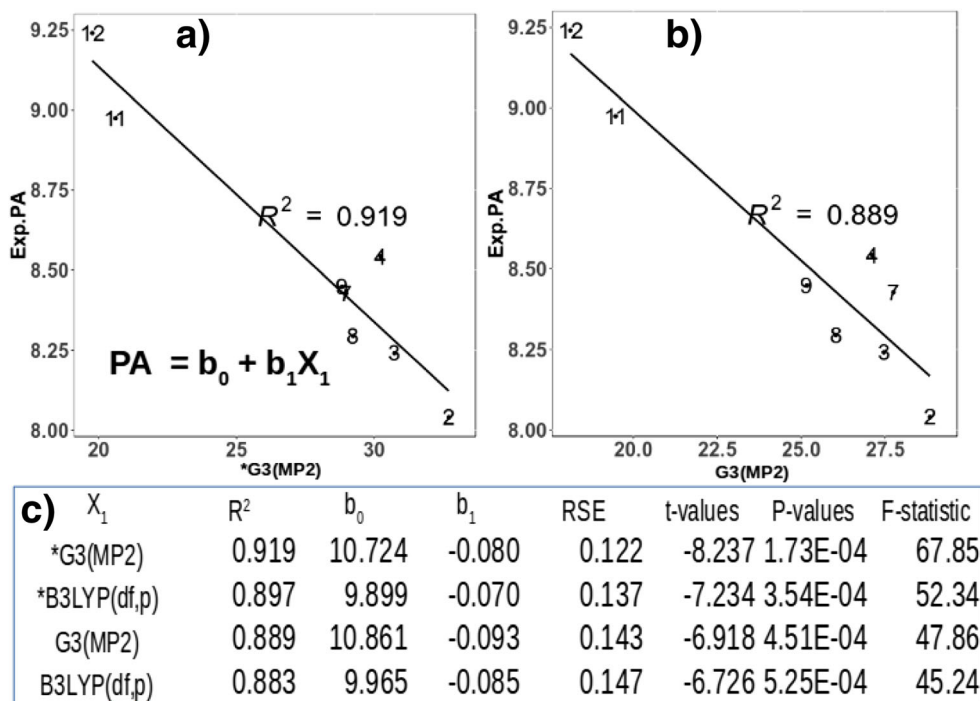
was found not to be the most reactive site [48–50]. The natural population analysis (NPA) of the atomic charges, $q(N)$, which was obtained from a M062X/6-311G(d,p) single point calculation on the B3LYP/6-31+G(d) optimized geometry, was used to calculate the Fukui indices, using the condensed Fukui functions of a j -atomic site for the electrophilic (f_j^-) or nucleophilic (f_j^+) or radical (f_j^0) attack:

$$f_j^- = q_j(N) - q_j(N-1)$$

$$f_j^+ = q_j(N+1) - q_j(N)$$

$$f_j^0 = \frac{1}{2} [q_j(N+1) - q_j(N-1)]$$

Fig. 9 The correlation of the experimental proton affinity (Exp-PA in eV) with the computed pK_a value, calculated by G3(MP2) and B3LYP(df,p) methods, in (a) acetonitrile (indicated by *) and (b) water as medium, with (c) the statistical analysis of these correlations



The centers for the Fukui electrophilic attack (f^-) of the molecules were obtained by subtracting the electronic density orbital of the cationic molecule (an $(N-1)$ electron system) from that of the neutral molecular orbital (N electron system), using Multiwfn [51, 52] multifunctional wavefunction analyzer (with iso-value 0.005). The nucleophilic attack (f^+) centers, on the other hand, were obtained by subtracting the electronic density orbital of the neutral molecule from that of the anionic molecular orbital (an $(N+1)$ electron system). The natural population analysis (NPA) is a good choice for the Fukui density surface, since it is able to differentiate the reactive site [48], though it also has a tendency to overestimate iconicity [53]. Another advantage of the NPA method is related to its insensitivity to the basis-set used, because of its application of the occupancy-weighted symmetric orthogonalization procedure, for transforming the non-orthogonal atomic orbitals into an orthogonal set [54]. The values of the Fukui indices of selected atoms in the molecules are in the supplementary material (Table S3), while the feature of their nucleophilic attack (tendency to accept electrons) and electrophilic attack (tendency to donate electrons) properties are shown in Fig. 10.

The atoms which represent the center for stronger nucleophilic attack (f^+) are the N and two O atoms of the NO_2 unit, and the para-carbon atoms of the benzene ring (Fig. 10 a). The two O atoms are the strongest center for the nucleophilic attack and their nucleophilic properties generally increase (larger f^+ value), as the electron donating tendency of the para-substituent R increases, in going from molecule 1 to 12. This evidently shows that in all 12 molecules the para-substituent R is strongly coupled with NO_2 , via strong electron communication through the benzene ring [3]. The calculated Fukui center for nucleophilic attack (f^+) being concentrated on the NO_2 group (Fig. 10 a) is in agreement with the fact that the electron involved in the first reduction of all molecules 1–12 is concentrated on the NO_2 group [3].

The ortho and the meta carbon atoms of the benzene ring in six of the molecules act as a very strong center of electrophilic attack (higher values of f^-), except in molecules 4, 6, 7, 10, 11, and 12, where the substituent atoms and/or para C carbon dominate the electrophilicity, as shown in Fig. 10b and also in Supplementary Table S3. The atoms that act as strong electrophilic centers were also observed to act as centers for radical attack (high f_j^0 values). Similarly, the two O atoms of the NO_2 group can also act as centers for radical attack.

Intra-molecular QTAIM properties

The quantum theory of atoms in molecules method (QTAIM) defines chemical bonding and structure of a chemical system, based on the topology of the electron density, expressed amongst others as four types of critical points, namely an atom

critical point, bond critical point, ring critical point, and cage critical point. The atom critical points define the position of atoms, and bond critical points define an existence of bonds. The values of the gradient of electron density ($\nabla\rho$) and its Laplacian ($\nabla^2\rho$) provide complementary information. A negative value of $\nabla^2\rho < 0$ is an indication that the bond is an open shell interaction, like covalent bonds, while a positive value of $\nabla^2\rho > 0$ depicts a closed shell interaction, such as hydrogen bonds [55].

The plots of the surface of $\nabla^2\rho$ are shown in Fig. 11, where the solid line regions represent regions of charge concentration ($\nabla^2\rho < 0$), which are analogous to the electron pairs in a Lewis structure [55], as in covalent bonds. Supplementary Table S4 lists the following values, for selected bonds involving atoms N, O, and F, namely: the electron density ($\nabla\rho$), its Laplacian ($\nabla^2\rho$), bond ellipticity (part of the indicators that determine the strength of bonds), the Laplacian of repulsive contribution to virial field (∇^2V_{rep} , also part of the indicators that determine the strength of bonds), internuclear distance (Δx), kinetic energy of electron (G), potential energy of electron (energy density (V)), and their ratio ($-G/V$). When the ratio $-G/V > 1$, it is indicative of a noncovalent interaction, but in the presence of covalent interactions, the ratio becomes smaller than unity ($-G/V < 1$) [56].

The correlation of the experimental reduction potential (E^0) with internuclear distance (note: not the same as electronic bond distance) of $\text{N}-\text{C}$ and $\text{N}=\text{O}$ for the NO_2 group in each of the 12 molecules, in their neutral ($R^2 = 0.843$) and reduced state ($R^2 = 0.565$), are shown in Supplementary Fig. S3. The internuclear distance (Δx) $_{\text{N}-\text{C}}$ is longer in the neutral molecules (2.74–2.80 Å) than in their reduced forms (2.63–2.71 Å), while (Δx) $_{\text{N}=\text{O}}$ is longer in the reduced form (2.39–2.45 Å) owing to the additional electron density than in the neutral molecules (2.32–2.34 Å) (see Table S4). Another interesting pattern is the gradual decrease in the $\text{N}-\text{C}$ internuclear distance of the neutral molecules from 1 to 12, while the $\text{N}=\text{O}$ bond gradually increases in the neutral molecules from 1 to 12. The implication is that as $\text{N}=\text{O}$ increases and $\text{N}-\text{C}$ decreases in length, owing to the increasing electron donating tendency of the para-substituent of the molecules from 1 to 12, their reduction potential simultaneously shifts toward more negative values, therefore progressively reducing the possibility of reduction.

The QTAIM properties ($\nabla\rho$, $\nabla^2\rho$, bond ellipticity, ∇^2V_{rep} , G , V , and $-G/V$) of these two bonds ($\text{N}-\text{C}$ and $\text{N}=\text{O}$) also demonstrate a similar pattern as shown in Supplementary Fig. S4. The values of the ρ , bond ellipticity, G , and ratio $-G/V$ of the $\text{N}-\text{C}$ bond generally are lower in the neutral state than in the reduced state of the molecules, with a gradual increase in their values from molecule 1 to 12, corresponding to the decrease in electron withdrawing ability of the R para-substituent, resulting in a progressive increase in shift of reduction potential to more negative values. The reverse was found for the values

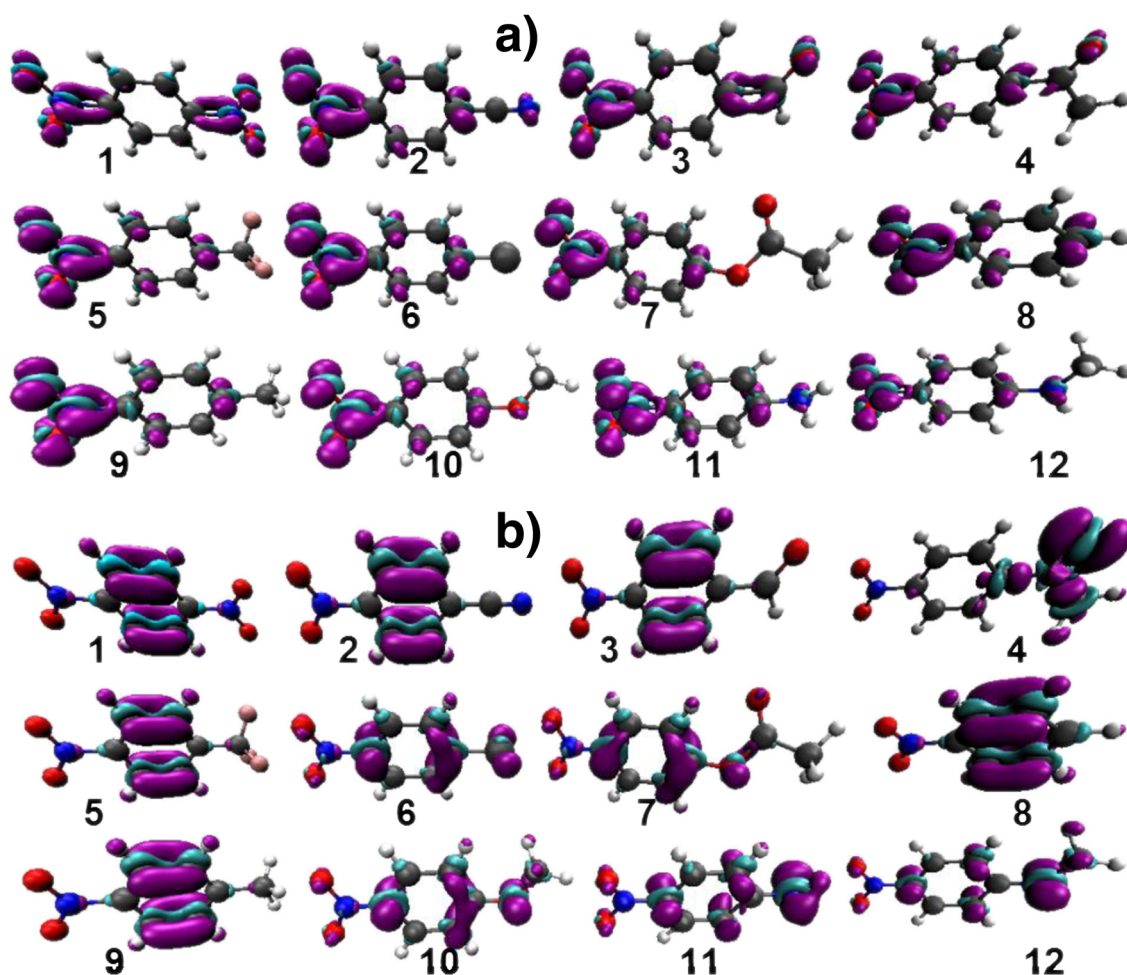


Fig. 10 The electronic density surface representative of the (a) Fukui center for nucleophilic attack (f^+), or the (b) Fukui center for electrophilic attack (f^-) of the 12 molecules, obtained using Multiwfn [51, 52] multifunctional wavefunction analyzer (iso-value 0.005)

of V and $\nabla^2\rho$ of the same N–C bonds, which are higher in the neutral than the reduced state, and decrease consistent with the decrease in electron withdrawing ability of the para-substituent R from molecule 1 to 12. In the reduced state, the change in these QTAIM internuclear bond properties of the N=O bond from molecule 1 to 12 is reasonably correlated with the gradual change in observed experimental reduction potential ($R^2 = 0.632\text{--}0.893$), more so than for the N–C bond properties ($R^2 = 0.057\text{--}0.769$). However, in the neutral state, the QTAIM properties of N–C are more correlated with the decreasing experimental reduction potential ($R^2 = 0.742\text{--}0.928$), than those of the N=O bond ($R^2 = 0.365\text{--}0.885$).

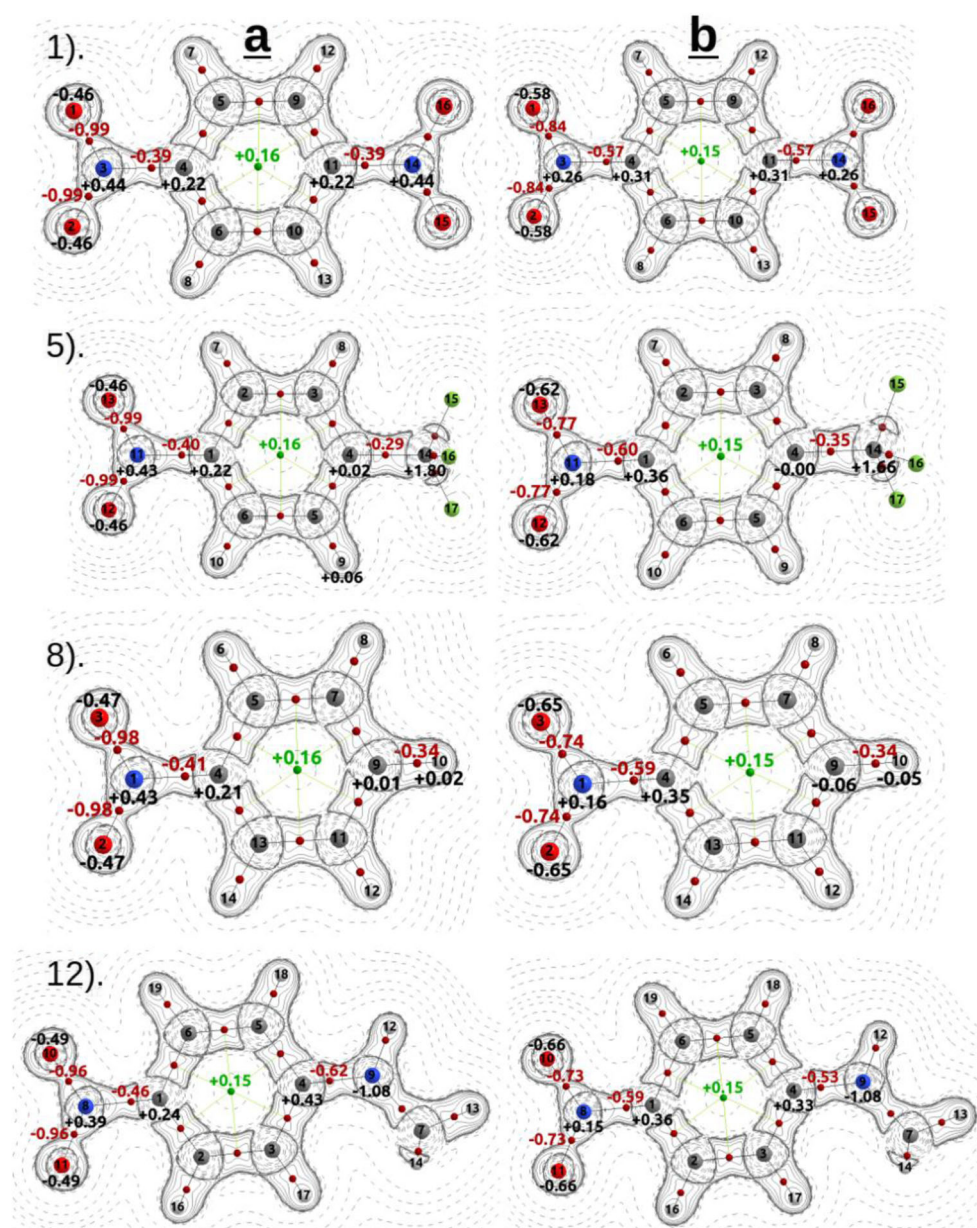
The properties of N=O show a trend directly opposite to the trend of the N–C internuclear bonds. The ρ , bond ellipticity, G , and ratio $-G/V$ values of the N=O internuclear bond are higher in the neutral state than in the reduced state of the molecules (gradual decrease in their values from molecule 1 to 12), while its V and $\nabla^2\rho$ of bonds are lower in the neutral than in the reduced state (increasing corresponding to the decrease in electron withdrawing R substituent from molecule 1

to 12). Evidently, an increase in the electron cloud around NO_2 , either as a result of moving from the neutral to reduced state, or as a result of the presence of a stronger electron donating group (in going from molecule 1 to 12), leads to a decrease in the internuclei bond distance of N–C, but an increase in Δx of N=O. This consequently leads to increasing internuclei bond strength of N–C, as is evident from the increasing values of ρ , bond ellipticity, G , and ratio $-G/V$ of the N–C internuclei bonds, simultaneously with lower values of V and $\nabla^2\rho$ (from the lower to higher electron cloud around NO_2), but to a weaker bond strength of N=O.

The values of ratio $-G/V$ show an appreciable correlation with $\nabla^2\rho$, especially in the reduced state of the molecules ($R^2 = 0.886$), as shown in Supplementary Fig. S5. The implication is that the stronger bonds are characterized with lower values of $\nabla^2\rho$ and ratio $-G/V$. The values of ratio $-G/V$ are within the range of covalent interaction, since $-G/V < 1$ [56].

The QTAIM atomic properties of the N, O, F, and Cl atoms in the molecules are supplied in Supplementary Table S5, showing the atomic charges (q), atomic Lagrangian (L),

Fig. 11 The representative structures of molecules 1, 5, 8, and 12, showing the plot of the Laplacian of the electron density ($\nabla^2\rho$ in $e a_0^{-5}$), the bond critical points (BCP), and some selected atomic charges and BCP values for (a) the neutral and (b) anionic molecules, using the QTAIM method as implemented in AIMAll

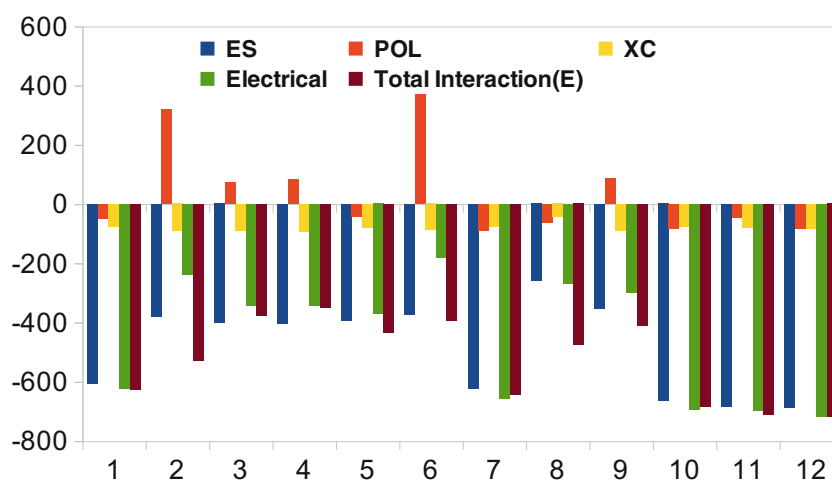


atomic electron kinetic (K), and the intra-atomic dipole moment ($|\mu_{\text{intra}}|$). The change in the atomic properties of the N atom of the NO_2 group, based on the effect of the para-substituents (R) on the reduction potential of the 12 molecules, is shown in Supplementary Fig. S6. The atomic charge of the N atom of the neutral molecule decreases, while its intra-atomic dipole increases from molecule 1 to 12 ($R^2 = 0.722$ to 0.895), as the reduction potential shifts to more negative values. In the reduced state, both the atomic charge and dipole moment of the N atoms decrease with the shift of reduction potential to more negative values. These reduced states are characterized with a higher intra-atomic dipole of N atoms, but lower atomic charges, when compared to the neutral states.

Natural energy decomposition analysis (NEDA)

Each of the 12 molecules is fragmented into three, as indicated in Fig. 1, where the common NO_2 group constitutes fragment one, the benzene ring is fragment two, and the para-substituent R is fragment three. The interaction between the fragments was studied using the natural energy decomposition analysis (NEDA, for details see the experimental section) which is an important concept that can be used to calculate the interacting energy of the fragments (ΔE) [29], in terms of their five components, namely, electrostatic (ES), charge transfer (CT), polarization (POL), exchange (XC), and electrical (EL) energy contributions, etc. The contribution of the five components ES, CT, POL, XC, and EL to the total interaction of the

Fig. 12 The feature of each contribution of the electrostatic (ES), polarization (POL), exchange energy (XC), and electrical (EL) energy components to the total interaction energy E (where $\Delta E = EL + CORE + CT$) of the three fragments in molecules 1 to 12. (where $CORE = XC + DEF - SE$; and DEF is the deformation energy of the perturbed wave function and SE is the self-energy correction). All energies are in kcal mol^{-1}



fragments (ΔE in kcal mol^{-1}) in each of the 12 molecules is given in Supplementary (Table S6) and the features of their changes are shown in Fig. 12, except for the contribution of CT. The order of the inter-fragment interactions (ΔE) of the molecules is as follows: $12 > 11 > 10 > 7 > 1 > 2 > 8 > 5 > 9 > 6 > 3 > 4$ according to the strength of their interactions in terms of ΔE . The stronger inter-fragment interactions in molecules like 12, 11, 10, 7, and 1 can be traced to their highly favorable electrical and electrostatic energies between the fragments. The inter-fragment polarization energy (POL) of molecules 2 and 6 is highly unfavorable (large positive value) for their inter-fragment interactions, but is compensated for by the molecules' most favorable CT values compared to the rest of the molecules (Table S6).

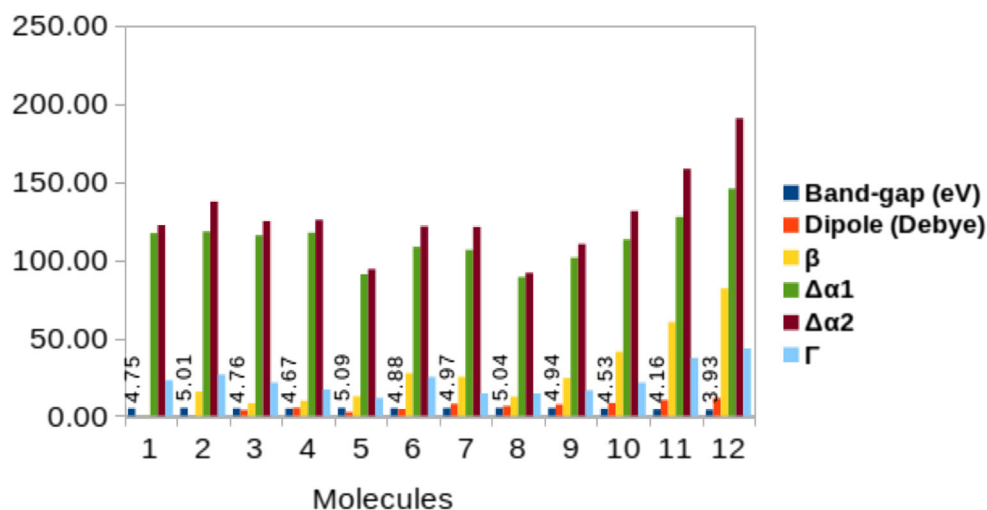
The induced energy (cp-def) and dipole moment of the three fragments in each of the molecules are shown in Supplementary Fig. S7, and the data are in Table S7. The induced energy (in kcal mol^{-1}) and dipole (in Debye) were calculated from the difference between the perturbed states (def) values (i.e., each fragment in the absence of the effect

of other fragments) and that of their values in the presence of other fragments (cp). All three fragments have a significant induced energy (between -1 and $-0.3 \text{ kcal mol}^{-1}$), while the induced dipole is only significant in the fragments of molecules 2, 3, 4, 5, 6, and 8, especially in their fragment three (para substituent R). The induced dipole of fragment one (NO_2) is insignificant in all the molecules (less than 0.06 Debye), except in molecule 6 with $R = p\text{-Cl}$ (0.61 Debye).

Molecular properties

Molecular properties, such as the molecular band gap, dipole, hyperpolarizability (β), first and second polarizabilities ($\Delta\alpha_1$, $\Delta\alpha_2$), and exaltation index (Γ) are shown in Fig. 13 and the values are given in Table S8. A higher value of hyperpolarizability (β) and exaltation index (Γ), accompanied with a lower band gap, was obtained in the molecules with electron donating para-substituents R (molecules 10, 11, and 12), while molecules 1 to 5, with electron withdrawing para-substituents, have lower hyperpolarizability (β), a lower

Fig. 13 The plot of the molecular band gap (in eV), dipole (in Debye), hyperpolarizability (β in esu), the first and second polarizabilities ($\Delta\alpha_1$, $\Delta\alpha_2$), and exaltation index (Γ) for all 12 nitrobenzene molecules



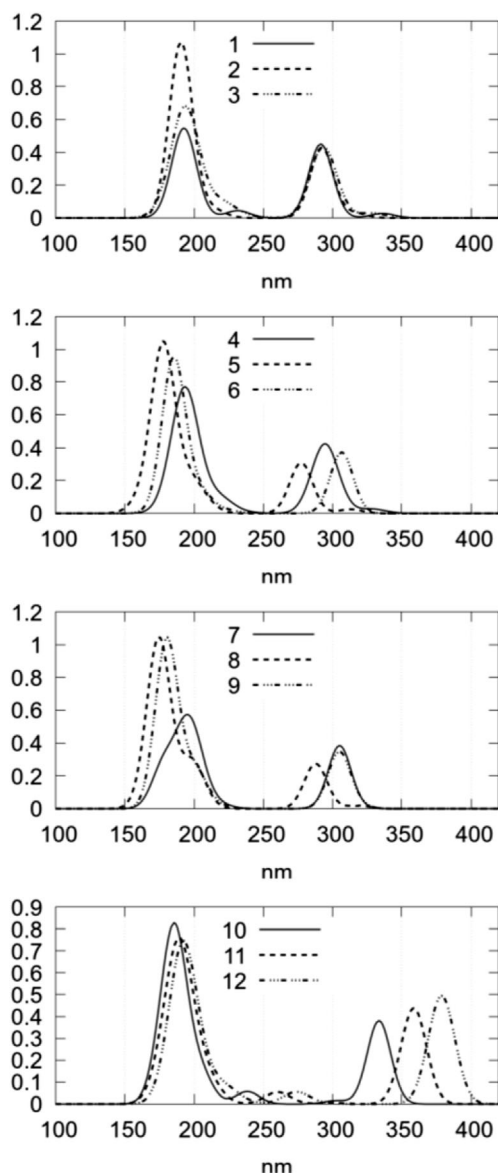


Fig. 14 The features of the wavelength (λ in nm) and strength (f) of the UV electron transitions in the molecules 1 to 12

exaltation index (Γ), and a higher band gap (Fig. 13). The results of the correlation of hyperpolarizability (β) with $\Delta\alpha_1$, $\Delta\alpha_2$, and Γ (Fig. S8) clearly show the gradual increase in the first and second polarizabilities and the exaltation index (Γ), as hyperpolarizability increases in value from molecule 1 to 12, according to the decrease in electron withdrawing tendency of the para-substituent R. A highly negative value of Γ indicates high stability, while a highly positive value means low stability, as has been used to estimate the stabilities of the atomic clusters and for the relative aromaticity [24, 57]. This implies that as the conducting strength of the molecule increases from 1 to 12 in terms of lower band gap, and as their possible application as nonlinear optical (NLO) materials increases in terms of higher hyperpolarizability values, their

stability decreases in terms of a higher positive value of the exaltation index (Γ).

A significant level of correlation was obtained when the computed values of the HOMO, LUMO, band gap, and dipole moment of the 12 molecules were correlated with the available experimental PA and IE values (Fig. S9). There was a gradual increase in the values of the HOMO, LUMO, and significant increase in the dipole moment, as the values of Exp-PA increased from molecule 1 to 12, but resulted in decreasing energy band gap. A reverse of this observation for PA was observed in the correlation of experimental IE with these molecular properties.

The UV excitation

The features of the UV excitation in the molecules are shown in Fig. 14, and the full description of the nature of the UV excitation peaks, in terms of the electron transition between the orbitals and the fragment contribution is in the supplementary material (Table S9). There is a gradual bathochromic shift of the peak above 250 nm to a progressively longer wavelength from molecule 1 to 12, as the strength of electron donation increases (Fig. 14). The bathochromic shift to a longer wavelength is in agreement with available experimental UV absorption maxima, as obtained from the NIST database [41], namely at $\lambda \approx$ ca. 260 nm for molecules 1 to 8, with the peak shifting to $\lambda = 320$ nm for molecule 10 and to $\lambda = 370$ nm for molecule 11. This provides further insight into the gradually increasing trend of electron conductivities and nonlinear optics (NLO) applicability. However, a hypsochromic shift (of the peak above 250 nm) to lower absorption values and shorter wavelength was observed from molecule 1 to 12.

The features of the HOMO (or H-1) to LUMO electron transfer in molecules, such as 1, 2, 3, 4, 5, and 6, with a slightly electron withdrawing para-substituent group R, predominantly occur from fragment two to fragment one (see Fig. 2), while a little also is transferred to fragment 3; however, very negligibly in molecules 5 and 6 (Table S9). In the molecules with a stronger electron donating group like 10, 11, and 12, the HOMO (or H-1) to LUMO electron excitation occurs from the contribution of both fragments two and three to fragment one. A very high percentage of electron transfer from the para-substituent R (fragment three) to NO_2 (fragment one) is further evidence of very strong electron coupling between the NO_2 group and the para-substituent R, via the aromatic benzene ring [3].

Conclusions

In this study, a new insight into the chemistry of 12 para-substituted nitrobenzene compounds was obtained, using

different computational methods. The optimized geometry of the molecules was obtained by DFT methods, and their properties were studied using the higher level computational method G3(MP2) and the DFT methods. The results obtained can be summarized as follows:

- Among the adopted DFT methods, M062X(6–311+G(2df,2p)) competitively reproduced the experimental reduction potentials to a very high accuracy (MAD = 0.048 V), to the same degree as the high-level computational method G3(MP2) (with MAD = 0.067 V), depending on the choice of the free energy circle used in the calculation of the reduction potential. Therefore, when G3(MP2) calculations become prohibitively expensive as the size of the molecule increases, affordable DFT methods can instead be used with confidence to calculate reduction potentials to a high level of accuracy.
- The high-level computational method G3(MP2) produced the best agreement with experimental electron affinities (MAD = 0.066 eV) and the DFT method B3LYP/6–311+G(df,p) the best agreement with experimental proton affinities (MAD = 0.125 eV).
- The benzene ring acts as a strong coupling link between the nitro and para-substituents. Therefore, increasing the electron donating ability of the para-substituent from molecule 1 to 12 resulted in a higher density electron cloud around NO₂, while reducing its susceptibility to further reduction consequently resulted in a lower, more negative reduction potential.
- The NO₂ group acts as the main center of chemical action for many of the observed chemical properties, in terms of reduction potential, proton affinity, etc., and was also found to be the most significant center for nucleophilic (f^+) attack, using Fukui indices.
- The strong electron coupling between the various para-substituents and the NO₂ group via the aromatic benzene ring was also confirmed through a higher percentage of electron excitation from the para-substituent of molecules 10, 11, and 12 (fragment 3) to the NO₂ group (fragment 1), which was accompanied by a bathochromic shift to a longer wavelength, as well as increasing polarizabilities, hyperpolarizabilities, a lowering of the band-gap, and increasing values of the exaltation index.
- The increasingly negative (lower) experimental reduction potential of the molecules from 1 to 12 was also accompanied by decreasing electron affinity and ionization energy, with simultaneously increasing proton affinity and consequently decreasing pK_a values.
- A gradual increase in HOMO and LUMO energies from molecules 1 to 12 was accompanied by a significant increase in the dipole moment but a decrease in energy band gap.

- The QAIM properties of the NO₂ group (such as bond lengths) change significantly with increasing electron cloud around NO₂, either owing to moving from the neutral state to the reduced state, or to the increase in electron donating tendency of the para-substituents from molecule 1 to 12, therefore resulting in increasingly longer internuclear N=O bonds (weakened) but decreasingly shorter N–C bonds (strengthened). These properties were also found to correlate significantly with the experimentally obtained reduction potentials of these 12 molecules.

Acknowledgments The authors would like to acknowledge the University of the Free State and the NRF in South Africa for financial support (Grant Nos: 109673, 113327 and 96111) and CHPC for the simulation facilities.

Compliance with ethical standards

Conflict of interest This work does not require any ethical statement and contains no conflict of interests.

Publisher's note Springer Nature remains neutral with regard to jurisdictional claims in published maps and institutional affiliations.

References

1. Smith WH, Bard AJ (1975) Electrochemical reactions of organic compounds in liquid ammonia. II. Nitrobenzene and nitrosobenzene. *J Am Chem Soc* 97:5203–5210. <https://doi.org/10.1021/ja00851a030>
2. Edwards DI (1986) Reduction of nitroimidazoles in vitro and DNA damage. *Biochem Pharmacol* 35:53–58. [https://doi.org/10.1016/0006-2952\(86\)90554-X](https://doi.org/10.1016/0006-2952(86)90554-X)
3. Kuhn A, Von Eschwege KG, Conradie J (2012) Reduction potentials of para - substituted nitrobenzenes—an infrared, nuclear magnetic resonance, and density functional theory study. *J Phys Org Chem* 25:58–68. <https://doi.org/10.1002/poc.1868>
4. Chowdhury S, Kebarl P (1986) Electron affinities of Di- and Tetracyanoethylene and Cyanobenzenes based on measurements of gas-phase Electron-transfer Equilibria. *J Am Chem Soc* 108:5453–5459. <https://doi.org/10.1021/ja00278a014>
5. Chowdhury S, Heinis T, Kebarl P (1986) Radical anions. Electron affinities of benzene, naphthalene, and anthracene having formyl, cyano, and nitro substituents. *J Am Chem Soc* 108:4662–4663. <https://doi.org/10.1021/ja00275a074>
6. Huh C, Kang CH, Lee HW et al (1999) Thermodynamic stabilities and resonance demand of aromatic radical anions in the gas phase. *Bull Chem Soc Jpn* 72:1083–1091. <https://doi.org/10.1246/bcsj.72.1083>
7. Muckerman JT, Skone JH, Ning M, Wasada-tsutsui Y (2013) Toward the accurate calculation of pKa values in water and acetonitrile ☆. *Biochim Biophys Acta* 1827:882–891. <https://doi.org/10.1016/j.bbapbio.2013.03.011>
8. Li X, Fu Y (2008) Theoretical study of reduction potentials of substituted flavins. *J Mol Struct* 856:112–118. <https://doi.org/10.1016/j.theochem.2008.01.029>
9. Pakiari AH, Siahrostami S, Mohajeri A (2008) Application of density functional theory for evaluation of standard two-electron reduction potentials in some quinone derivatives. *J Mol Struct*

- THEOCHEM 870:10–14. <https://doi.org/10.1016/j.theochem.2008.08.030>
10. Marenich AV, Ho J, Coote ML et al (2014) Computational electrochemistry: prediction of liquid-phase reduction potentials. *Phys Chem Chem Phys* 16:15068–15106. <https://doi.org/10.1039/c4cp01572j>
 11. Jono R, Yamashita K (2015) A method to calculate redox potentials relative to the normal hydrogen electrode in nonaqueous solution by using density functional theory-based. *Phys Chem Chem Phys* 17: 27103–27108. <https://doi.org/10.1039/C5CP05029D>
 12. Liptak MD, Shields GC (2001) Accurate p K a calculations for carboxylic acids using complete basis set and Gaussian-n models combined with CPCM continuum solvation methods. *J Am Chem Soc* 123:7314–7319. <https://doi.org/10.1021/ja010534f>
 13. Perez-Gonzalez A, Galano A (2011) Ionization energies, proton affinities, and p K a values of a large series of Edaravone derivatives: implication for their free radical scavenging activity. *J Phys Chem B* 115:10375–10384. <https://doi.org/10.1021/jp2047163>
 14. Namazian M, Lin CY, Coote ML (2010) Benchmark calculations of absolute reduction potential of Ferricinium / Ferrocene couple in nonaqueous solutions. *J Chem Theory Comput* 6:2721–2725. <https://doi.org/10.1021/ct1003252>
 15. Henry DJ, Sullivan MB, Radom L et al (2003) G3-RAD and G3X-RAD: modified Gaussian-3 (G3) and Gaussian-3X (G3X) procedures for radical thermochemistry G3-RAD and G3X-RAD : modified Gaussian-3 “G3 ... and Gaussian-3X” G3X ... procedures for radical thermochemistry. *J Chem Phys* 118:4849–4860. <https://doi.org/10.1063/1.1544731>
 16. Henry DJ, Sullivan MB, Radom L et al (2007) G3-RAD and G3X-RAD : modified Gaussian-3 “G3 ... and Gaussian-3X” G3X ... procedures for radical thermochemistry. *J Chem Phys* 3:4849–4860. <https://doi.org/10.1063/1.1544731>
 17. Fu Y, Liu L, Yu H et al (2005) Quantum-chemical predictions of absolute standard Redox potentials of diverse organic molecules and free radicals in Acetonitrile. *J Am Chem Soc* 127:7227–7234. <https://doi.org/10.1021/ja0421856>
 18. Zhan C, Dixon DA (2001) Absolute hydration free energy of the proton from first-principles electronic structure calculations. *J Phys Chem A* 105:11534–11540
 19. Camaioni DM, Schwerdtfeger CA (2005) Of H+, OH-, and H3O+. *J Phys Chem A* 109:10795–10797. <https://doi.org/10.1021/jp054088k>
 20. Kelly CP, Cramer CJ, Truhlar DG (2007) Single-ion solvation free energies and the normal hydrogen electrode potential in methanol, acetonitrile, and dimethyl sulfoxide. *J Phys Chem B* 111:408–422. <https://doi.org/10.1021/jp0654031>
 21. Hunter EPL, Lias SG, Hunter EPL, Lias SG (1998) Evaluated gas phase Basicities and proton affinities of molecules: an update evaluated gas phase Basicities and proton affinities of molecules: an update. *J Phys Chem Ref Data* 27:413–656
 22. Fifen JJ, Dhaouadi Z, Nsangou M (2014) Revision of the thermodynamics of the proton in gas phase. *J Phys Chem A* 118:11090–11097. <https://doi.org/10.1021/jp508968z>
 23. Alparone A (2012) Dipole (hyper)polarizabilities of fluorinated benzenes: an ab initio investigation. *J Fluor Chem* 144:94–101. <https://doi.org/10.1016/j.jfluchem.2012.07.016>
 24. de Silva IC, de Silva RM, Nalin de Silva KM (2005) Investigations of nonlinear optical (NLO) properties of Fe, Ru and Os organometallic complexes using high accuracy density functional theory (DFT) calculations. *J Mol Struct THEOCHEM* 728:141–145. <https://doi.org/10.1016/j.theochem.2005.02.092>
 25. Mendes PJ, Ramalho JPP, Candeias AJE et al (2005) Density functional theory calculations on eta(5)-monocyclopentadienylnitrilecobalt complexes concerning their second-order nonlinear optical properties. *J Mol Struct* 729:109–113. <https://doi.org/10.1016/j.theochem.2004.12.048>
 26. Liu Y, Liu C-G, Sun S-L et al (2012) Redox-switching second-order nonlinear optical responses of N⁺N⁺ ruthenium complexes. *Comput Theor Chem* 979:112–118. <https://doi.org/10.1016/j.comptc.2011.10.025>
 27. The CTCP table of experimental and calculated static dipole polarizabilities for the electronic ground states of the neutral elements. In: *Cent. Theor. Chem. Physics, New Zeal. Inst. Adv. Study, Massey Univ. (Albany Campus), New Zeal.* <http://ctcp.massey.ac.nz/index.php?menu=dipole&page=dipole>. Accessed 24 Oct 2018
 28. Kazuo K, Keiji M (2004) A new energy decomposition scheme for molecular interactions within the Hartree-Fock approximation. *Int J Quantum Chem* 10:325–340. <https://doi.org/10.1002/qua.560100211>
 29. Glendening ED, Streitwieser A (1994) Natural energy decomposition analysis: an energy partitioning procedure for molecular interactions with application to weak hydrogen bonding, strong ionic, and moderate donor – acceptor interactions. *Natural energy decomposition analysis: an energy par. J Chem Phys* 100:2900–2909. <https://doi.org/10.1063/1.466432>
 30. Zhao Y, Truhlar DG (2006) A new local density functional for main-group thermochemistry, transition metal bonding, thermochemical kinetics, and noncovalent interactions. A new local density functional for main-group thermochemistry, transition metal bonding, thermochemical kin. *J Chem Phys* 125:194101. <https://doi.org/10.1063/1.2370993>
 31. Marenich AV, Cramer CJ, Truhlar DG (2009) Universal Solvation model based on solute Electron density and on a continuum model of the solvent defined by the bulk dielectric constant and atomic surface tensions. *J Phys Chem B* 113:6378–6396
 32. Skyner RE, Mcdonagh JL, Groom CR, Van Mourik T (2015) A review of methods for the calculation of solution free energies and the modelling of systems in solution. *Phys Chem Chem Phys* 17: 6174–6191. <https://doi.org/10.1039/C5CP00288E>
 33. Frisch MJ, Trucks GW, Schlegel HB et al (2009) Gaussian 09
 34. Glendening ED, Badenhop JK, Reed AE et al (2013) NBO 6.0
 35. Helms V, Winstead C, Langhoff P (2000) Low-lying electronic excitations of the green fluorescent protein chromophore. *J Mol Struct THEOCHEM* 506:179–189. [https://doi.org/10.1016/S0166-1280\(00\)00411-5](https://doi.org/10.1016/S0166-1280(00)00411-5)
 36. Schmidt MW, Baldrige KK, Boatz JA et al (1993) General atomic and molecular electronic structure system. *J Comput Chem* 14: 1347–1363
 37. Humphrey W, Dalke A, Schulten K (1996) VMD: visual molecular dynamics. *J Mol Graph* 14:27–28-38
 38. Pettersen EF, Goddard TD, Huang CC et al (2004) UCSF chimera—a visualization system for exploratory research and analysis. *J Comput Chem* 25:1605–1612. <https://doi.org/10.1002/jcc.20084>
 39. Keith TA (2017) AIMAll
 40. (2018) The R Core Team: a language and environment fo statistical computing
 41. Linstrom PJ, Mallard WG, Eds. NIST Chemistry WebBook, NIST Standard Reference Database Number 69, National Institute of Standards and Technology, Gaithersburg
 42. Mock RS, Grimmsrud EP (1989) Gas-phase electron photodetachment spectroscopy of the molecular anions of nitroaromatic hydrocarbons at atmospheric pressure. *J Am Chem Soc* 111:2861–2870. <https://doi.org/10.1021/ja00190a020>
 43. Chowdhury S, Kishi H (1989) Electron affinities of substituted nitrobenzenes. *Can J Chem* 67:603–610
 44. Martinsen DP (1976) Determination of the site of protonation of substituted benzenes in water chemical. *Org Mass Spectrom* 11: 762–772
 45. Lide D (2007) CRC handbook of chemistry and physics, 88th edn. CRC Press, Taylor & Francis, Boca Raton
 46. Mineva T, Parvanov V, Petrov I et al (2001) Fukui indices from perturbed Kohn-sham Orbitals and regional softness from Mayer

- atomic valences. *J Phys Chem A* 105:1959–1967. <https://doi.org/10.1021/jp003458w>
47. Millefiori S, Alparone A (1998) (hyper)polarizability conventional of chalcogenophenes C₄H₄X (X = O, S, se, Te) ab initio and density functional theory study. *J Mol Struct* 1280:59–78
48. Ja SA, Kolandaivel P (1997) Condensed Fukui function: dependency on atomic charges. *Mol Phys* 90:55–62. <https://doi.org/10.1080/002689797172868>
49. Gazquez JL, Mendez F (1994) The hard and soft acids and bases principle: an atoms in molecules viewpoint. *J Phys Chem* 98:4591–4593. <https://doi.org/10.1021/j100068a018>
50. Mendez F, Gazquez JL (1994) Chemical reactivity of enolate ions: the local hard and soft acids and bases principle viewpoint. *J Am Chem Soc* 116:9298–9301. <https://doi.org/10.1021/ja00099a055>
51. Lu T, Chen F (2012) Multiwfn: a multifunctional wavefunction analyzer. *J Comput Chem* 33:580–592. <https://doi.org/10.1002/jcc.22885>
52. Lu T, Chen F (2012) Quantitative analysis of molecular surface based on improved marching Tetrahedra algorithm. *J Mol Graph Model* 38:314–323. <https://doi.org/10.1016/j.jmgl.2012.07.004>
53. Sannigrahi AB, Nandi PK, Schleyer PR (1993) Ab initio theoretical study of the electronic structure, stability and bonding of dialkali halide cations. *Chem Phys Lett* 204:73–79. [https://doi.org/10.1016/0009-2614\(93\)85607-P](https://doi.org/10.1016/0009-2614(93)85607-P)
54. Reed AE, Weinstock RB, Weinhold F (1985) Natural population analysis. *J Chem Phys* 83:735–746
55. Calhorda MJ, Lopes PEM (2000) An “atoms in molecules” (AIM) analysis of the dihydrogen bond in organometallic compounds. *J Organomet Chem* 609:53–59. [https://doi.org/10.1016/S0022-328X\(00\)00235-7](https://doi.org/10.1016/S0022-328X(00)00235-7)
56. Solimannejad M, Malekani M, Alkorta I (2010) Theoretical study of the halogen-hydride complexes between XeH₂ and carbon halogenated derivatives. *J Mol Struct THEOCHEM* 955:140–144. <https://doi.org/10.1016/j.theochem.2010.06.004>
57. Liyanage PS, de Silva RM, de Silva KMN (2003) Nonlinear optical (NLO) properties of novel organometallic complexes: high accuracy density functional theory (DFT) calculations. *J Mol Struct THEOCHEM* 639:195–201. <https://doi.org/10.1016/j.theochem.2003.08.009>